A&A 647, A72 (2021)
https://doi.org/10.1051/0004-6361/202039196

Astronomy & Astrophysics

A new measurement of the Hubble constant using Type Ia supernovae calibrated with surface brightness fluctuations

Nandita Khetan[1,2], Luca Izzo[3], Marica Branchesi[1,2,4], Radosław Wojtak[3], Michele Cantiello[4], Chandrashekar Murugeshan[5], Adriano Agnello[3], Enrico Cappellaro[6], Massimo Della Valle[7], Christa Gall[3], Jens Hjorth[3], Stefano Benetti[6], Enzo Brocato[4,8], Jamison Burke[9,10], Daichi Hiramatsu[9,10], D. Andrew Howell[9,10], Lina Tomasella[6], and Stefano Valenti[11]

[1] Gran Sasso Science Institute, Viale F. Crispi 7, 67100 LAquila, AQ, Italy
e-mail: nandita.khetan@gssi.it
[2] INFN, Laboratori Nazionali del Gran Sasso, 67100 Assergi, Italy
[3] DARK, Niels Bohr Institute, University of Copenhagen, Jagtvej 128, 2200 Copenhagen, Denmark
[4] INAF, Osservatorio Astronomico d'Abruzzo, Via Mentore Maggini, Teramo 64100, Italy
[5] Centre for Astrophysics and Supercomputing, Swinburne University of Technology, Hawthorn, Victoria 3122, Australia
[6] INAF, Osservatorio Astronomico di Padova, Vicolo dell'Osservatorio 5, 35122 Padova, Italy
[7] INAF, Osservatorio Astronomico di Capodimonte, Salita Moiariello 16, 80131 Naples, Italy
[8] INAF, Osservatorio Astronomico di Roma, Via Frascati 33, 00040 Monte Porzio Catone, RM, Italy
[9] Las Cumbres Observatory, Goleta, CA 93117, USA
[10] Department of Physics, University of California, Santa Barbara, CA 93106, USA
[11] Department of Physics, University of California, 1 Shields Avenue, Davis, CA 95616-5270, USA

Received 17 August 2020 / Accepted 20 January 2021

ABSTRACT

We present a new calibration of the peak absolute magnitude of Type Ia supernovae (SNe Ia) based on the surface brightness fluctuations (SBF) method, aimed at measuring the value of the Hubble constant. We build a sample of calibrating anchors consisting of 24 SNe hosted in galaxies that have SBF distance measurements. Applying a hierarchical Bayesian approach, we calibrate the SN Ia peak luminosity and extend the Hubble diagram into the Hubble flow by using a sample of 96 SNe Ia in the redshift range $0.02 < z < 0.075$, which was extracted from the Combined Pantheon Sample. We estimate a value of $H_0 = 70.50 \pm 2.37$ (stat.) ± 3.38 (sys.) km s^{-1} Mpc^{-1} (i.e., 3.4% stat., 4.8% sys.), which is in agreement with the value obtained using the tip of the red giant branch calibration. It is also consistent, within errors, with the value obtained from SNe Ia calibrated with Cepheids or the value inferred from the analysis of the cosmic microwave background. We find that the SNe Ia distance moduli calibrated with SBF are on average larger by 0.07 mag than those calibrated with Cepheids. Our results point to possible differences among SNe in different types of galaxies, which could originate from different local environments and/or progenitor properties of SNe Ia. Sampling different host galaxy types, SBF offers a complementary approach to using Cepheids, which is important in addressing possible systematics. As the SBF method has the ability to reach larger distances than Cepheids, the impending entry of the *Vera C. Rubin* Observatory and JWST into operation will increase the number of SNe Ia hosted in galaxies where SBF distances can be measured, making SBF measurements attractive for improving the calibration of SNe Ia, as well as in the estimation of H_0.

Key words. supernovae: general – distance scale – cosmology: observations

1. Introduction

The standard cosmological model, also known as the Λ cold dark matter (ΛCDM) model, represents the only model that is consistent with a wide set of observations from different epochs of the Universe. This concordance model describes our Universe as flat, accelerating, and primarily composed of radiation, baryons, dark matter, and dark energy, with the latter two components being the most dominant, albeit elusive, constituents at the present time. One of the fundamental parameters governing the ΛCDM model is the Hubble constant (H_0), which sets the absolute scale of the Universe and can be measured both at early epochs, by the size of the sound horizon from the cosmic microwave background (CMB, Planck Collaboration XIII 2016; Bennett et al. 2013), and in the local present-time Universe using luminosity distance indicators (Freedman et al. 2001; Sandage et al. 2006; Riess et al. 2016). Comparing the absolute scale at the two opposite ends of the expanding Universe provides a stringent test of the standard cosmological paradigm.

With extensive ongoing efforts, H_0 measurements are achieving remarkable accuracy and precision at both of these extremes. In the local Universe, one of the most reliable measurements of H_0 comes from supernovae type Ia (SNe Ia), which however rely on primary distance indicators for their zero-point calibration (e.g., Cepheids and geometrical distances). The last couple of decades have witnessed gradual improvements in H_0 measurements using SNe Ia (e.g., Freedman et al. 2009, 2012; Riess et al. 2011, 2016; Dhawan et al. 2018; Phillips et al. 2019), with the most recent estimate by Riess et al. (2019), who obtained $H_0 = 74.03 \pm 1.42$ km s^{-1} Mpc^{-1} using the Cepheid calibration of SNe Ia (SH0ES program). Other powerful astrophysical probes measuring H_0 include time-delay gravitational lensing (e.g., Suyu et al. 2017; Birrer et al. 2019), the Tully–Fisher relation (e.g., Sorce et al. 2013), surface brightness

fluctuations (SBF; e.g., Jensen et al. 2001; Cantiello et al. 2018a), and the distance measurement using gravitational wave signals from binary compact objects (Abbott et al. 2017), to name a few.

The latest estimate of the Hubble constant based on CMB observations by the *Planck* satellite is $H_0 = 67.4 \pm 0.5\,\mathrm{km\,s^{-1}\,Mpc^{-1}}$ (Planck Collaboration VI 2020). Another way of estimating H_0 is through measurements of fluctuations in the matter density called baryon acoustic oscillations (BAOs, Cole et al. 2005; Eisenstein et al. 2005; Aubourg et al. 2015; Alam et al. 2017). The absolute calibration of BAOs is based on prior knowledge of the sound horizon size, which depends on the early-time physics, in turn making it dependent on the CMB. Macaulay et al. (2019) measured a value of $H_0 = 67.77 \pm 1.30\,\mathrm{km\,s^{-1}\,Mpc^{-1}}$ using BAOs and SNe Ia from the Dark Energy Survey (DES), where the absolute distance measurements from the BAOs were used to calibrate the intrinsic magnitude of the SNe Ia. This "inverse" distance ladder approach, where the distance calibration is done through CMB or other high-redshift observations, is not a direct method; it requires a cosmological model to build on.

The majority of the local independent methods, and combinations thereof, used to estimate H_0 stand in tension with the H_0 values inferred from the CMB analysis, with discrepancies ranging between 4σ and 6σ (Verde et al. 2019). However, a recent calibration of SNe Ia using the tip of the red giant branch (TRGB) method in the color-magnitude diagram of host galaxies of SNe Ia provided $H_0 = 69.8 \pm 0.8\,(\pm 1.1\%\,\mathrm{stat.}) \pm 1.7\,(\pm 2.4\%\,\mathrm{sys.})\,\mathrm{km\,s^{-1}\,Mpc^{-1}}$ (Freedman et al. 2019). Using a different calibration of the TRGB in the Large Magellanic Cloud (LMC), Yuan et al. (2019) estimated $H_0 = 72.4 \pm 2.0\,\mathrm{km\,s^{-1}\,Mpc^{-1}}$. After a reanalysis of the LMC TRGB extinction, Freedman et al. (2020) confirmed their earlier estimate of $H_0 = 69.6 \pm 0.8\,(\pm 1.1\%\,\mathrm{stat.}) \pm 1.7\,(\pm 2.4\%\,\mathrm{sys.})\,\mathrm{km\,s^{-1}\,Mpc^{-1}}$, which sits between the *Planck*-CMB value and the one resulting from SNe Ia calibrated using Cepheids.

If the difference between local H_0 measurements and the *Planck*-CMB measurement is statistically confirmed by future independent observations and analyses, it would hint at a possible inadequacy of the standard ΛCDM model and in turn imply the existence of some "new physics" beyond it, which would include new species of relativistic particles, nonzero curvature, dark radiation, or even a modification of the equations of general relativity (e.g., Bernal et al. 2016; Mörtsell & Dhawan 2018; Verde et al. 2019; Knox & Millea 2020). However, many modifications of the ΛCDM model appear in conflict with other existing cosmological tests and worsen the model fit to the observed CMB power spectrum (Arendse et al. 2020; Hill et al. 2020). Neither new physics nor identifiable systematics are currently able to resolve the tension. In this scenario, new and independent H_0 estimates and a credible quantification of the systematic uncertainties (instrumental and astrophysical) are necessary.

Among Hubble flow distance indicators, SNe Ia are the most reliable probes for H_0 measurement. In the cosmic distance ladder approach, SN Ia distances generally rely on some primary distance measurements in the nearby Universe, such as Cepheids (Riess et al. 2019) or the aforementioned TRGB. The ladder approach to estimating H_0 consists of three main steps: (1) absolute calibration of the primary distance indicator with geometric anchors, for example using parallaxes for Milky Way Cepheids (Gaia Collaboration 2018) and/or for LMC Cepheids, detached eclipsing binaries (DEBs; Pietrzyński et al. 2019), and masers (Riess et al. 2016); (2) calibrating the luminosity of nearby SNe Ia using the distance from the primary indicator to host galaxies of SNe Ia, and (3) using the calibrated relation between SN Ia light curve properties and luminosity to measure distances to SNe Ia in the Hubble flow. Therefore, to obtain accurate distances and H_0 estimates, it is necessary to control the various systematic errors arising in each of the above steps in order to gather a statistically significant sample of galaxies that host SNe Ia in the local Universe to be used as calibrators, as well as to have accurate distance estimates to the galaxies of this calibrating sample via primary distance methods.

Presently, the "yardstick" measurement, which highlights the Hubble tension in finding a higher H_0 with respect to early-Universe estimates, is based on the calibration that uses the Cepheid distance scale, in particular with Weisenheit magnitudes (Madore & Freedman 1991). This calibration currently relies on a sample of 19 nearby galaxies that host SNe Ia and whose distances are measured with Cepheids (SH0ES sample, Supernovae H_0 for the Equation of State of Dark energy, Riess et al. 2005, 2019). On the other hand, the H_0 estimate based on a sample of 18 SNe Ia whose distances to their host galaxies have been measured with the TRGB method shows a lower value of the Hubble constant, which is in agreement at the 1.2σ level with the *Planck* estimate (Freedman et al. 2020). In the wake of these results, it is imperative to exploit different methods to estimate precise distances in the local Universe in order to confirm or resolve the Hubble tension.

In this context, this work aims at exploring the use of the SBF distance method as an anchor for measuring distances to host galaxies of SNe Ia in the Hubble flow. Ajhar et al. (2001) compared SBF distances of galaxies hosting a SN Ia with their SN distance calibrated using Cepheids and homogenized the SBF and SN distance scales. Based on this result, we propose, for the first time, to calibrate SN Ia luminosity using SBF distances to their host galaxies, with the main goal of estimating the Hubble constant.

The possibility to measure accurate distances to early-type galaxies (and sometimes bulges of spiral galaxies) in the nearby Universe with SBF was first introduced by Tonry & Schneider (1988). Detailed descriptions about the SBF methods are given in Blakeslee et al. (1999, 2009), Biscardi et al. (2008). The SBF method determines the intrinsic variance in a galaxy image resulting from stochastic variations in the numbers and luminosities of the stars falling within the individual pixels of the image. The measured variance is normalized by the local galaxy surface brightness and then converted to the apparent SBF magnitude $\overline{m}$. The distance modulus, $\mu = \overline{m} - \overline{M}$, is then obtained knowing the absolute SBF magnitude $\overline{M}$, which depends on the stellar population properties (Blakeslee et al. 2001; Mei et al. 2005; Cantiello et al. 2018b). The $\overline{M}$ zero-point is tied directly to the Cepheid distance scale (empirical calibration, e.g., Tonry et al. 2001) or derived from stellar population models (theoretical calibration, e.g., Brocato et al. 1998; Cantiello et al. 2003; Raimondo et al. 2005; Marín-Franch & Aparicio 2006; Biscardi et al. 2008). The stellar populations dominated by evolved stars (with the red giant branch mostly contributing to the flux variance) make early-type galaxies ideal for estimating distances through SBF measurements (Blakeslee 2012). The SBF technique enables us to measure distances with a precision of 5–10% up to ∼100 Mpc with the current observatories, such as the *Hubble* Space Telescope (HST; Jensen et al. 2015).

Although the SBF distances are calibrated themselves using Cepheids, and represent a secondary calibrator method for SNe Ia, they offer potential advantages and useful insights in terms of

identifying possible systematic effects associated with the luminosity calibration. While SNe calibrated with Cepheids, such as the ones in the SH0ES sample, are all hosted in late-type galaxies, the SBF distance measurements are available mainly for early-type host galaxies, making SBF calibrator sample complementary, in terms of SN hosts, to the Cepheid sample. The comparison among the SBF and Cepheid calibrations enables us to identify possible systematics for luminosities of SNe Ia in different host galaxy types (Kang et al. 2020). Furthermore, early-type galaxies have generally less dust when compared with late-type galaxies, and hence the host extinction, which remains a challenge for SN light curve analysis (Tripp 1998; Burns et al. 2014; Brout & Scolnic 2020), is reduced. The distance range covered by SBF measurements significantly exceeds the one covered by the TRGB and Cepheid measurements, which helps to augment the number of calibrators. In terms of observational advantages, SBF can be measured on images that do not require the high resolution and depth necessary to resolve stellar photometry as for TRGB and Cepheids. Furthermore, this method does not require periodic observations of the galaxies.

The paper is organized as follows. In Sect. 2, we describe the nearby SN samples used as calibrators and the distant cosmological sample used for H_0 measurement. In Sect. 3, we explain the details of our analysis, and in Sect. 4, we present the Hubble diagram and our estimates of the Hubble constant. In Sect. 5, we evaluate the influence of the host galaxy type on the SN Ia standardization by applying a galaxy stellar-mass correction. Section 6 compares the distance measurements obtained by applying the SBF and Cepheid calibrations. We discuss our results in Sect. 7, and we draw our conclusions and discuss future prospects in Sect. 8.

2. Data

The choice and number of calibrators are key factors in defining the zero-point of the calibrating relation and eventually the accuracy of Hubble flow distance estimates, given that they determine the uncertainty on the H_0 value. In order to appropriately calibrate the peak luminosity of SNe Ia with SBF distance indicators, we first identified all the galaxies that host a SN Ia and have a distance measurement evaluated through the SBF technique. Then, we filtered this sample according to specific SN Ia data quality criteria, which are reported below.

2.1. SBF calibration sample

In order to build the SBF calibration sample, we cross-matched the major published SBF distance catalogs (Tonry et al. 2001; Ajhar et al. 2001; Jensen et al. 2003; Mei et al. 2003; Cantiello et al. 2007, 2013, 2018b; Blakeslee et al. 2009) with the SN catalog from Guillochon et al. (2017) available on the Open Supernova Catalog webpage[1]. The preliminary cross-matched sample consists of 45 galaxies. For the galaxies in this preliminary sample that have multiple SBF distance estimates, we selected the most recent SBF distance estimate, favoring the use of the HST data when available.

Taking into account the importance of the quality of the data of SN light curves (LC) for a good calibration, we applied LC quality cuts in order to avoid any systematics caused by their observed properties. Our fiducial calibration sample consists of SNe Ia with: (1) data in B and V bands with high cadence observations especially around the maximum and within the first 40 days after the peak brightness, in order to accurately sample the LC evolution and constrain the peak magnitude; (2) regular light curve shape (removing fast decliners with $s_{BV} < 0.5$, see Sect. 3 for the definition of the color-stretch parameter s_{BV}); and (3) low reddening (color $m_B - m_V < 0.3$ mag). Throughout this paper (except where differently indicated), $m_B - m_V$ refers to the pseudocolor derived from the maximum flux in the B and the V bands. Among the 45 SNe Ia in the preliminary sample, 24 of them pass the above selection criteria and form our final SBF calibration sample.

For the photometry of the SNe in our calibration sample, the optical (B and V band) light curves are taken from the published data assembled in Guillochon et al. (2017). The individual references for the photometric data of each object are given in Table A.1. Table 1 shows the SBF calibration sample listing the 24 SNe Ia selected to have high quality photometric data and standard light curve evolution. It lists the SN name (Col. 1), the host galaxy name (Col. 2), the SBF distance modulus along with the associated error (Cols. 3 and 4), the galaxy morphological type (Col. 5), the reference for the galaxy SBF distance (Col. 6) and the host galaxy stellar mass along with the error (Cols. 7 and 8). The stellar mass for each SN host galaxy used in this work is computed using the K_s-band magnitude from the 2MASS survey (Skrutskie et al. 2006) as described in Appendix B.

All the SBF distances used in the present paper are tied to a common empirical zero-point based on the results of the HST Key Project (KP) Cepheid distances by Freedman et al. (2001, hereafter F01) as described in Blakeslee et al. (2002). F01 adopt the Cepheid Period–Luminosity (P–L) relations by Udalski et al. (1999), and the metallicity corrections to the Cepheid distances by Kennicutt et al. (1998). The SBF zero-point calibration adopted by Tonry et al. (2001) was based on a previous estimate evaluated using six galaxies with KP Cepheid distances (Ferrarese et al. 2000) and needed a revision. A general correction formula for the published distances in Tonry et al. (2001) is provided by Blakeslee et al. (2010). This formula includes both the zero-point and second-order bias correction, which takes into account the variation of the data quality. All the distances from Tonry et al. (2001) in this work are corrected according to this formula bringing them to the same zero-point of the other SBF measurements in the present sample.

It is worth noting that our SBF distances are calibrated to the Cepheid zero-point based on Cepheid distances by F01, who adopted an LMC distance modulus of 18.50 ± 0.10 mag. Riess et al. (2016) for the Cepheid distances of the SNe Ia in the SH0ES sample (described in the next subsection) used a LMC distance of 18.493 ± 0.008 (stat.) ± 0.047 (sys.) mag based on 8 DEBs (Pietrzyński et al. 2013). The most recent value by Pietrzyński et al. (2019), which is anchored on 20 DEB stars in the LMC, gives $\mu_{\rm LMC} = 18.477 \pm 0.004$ (stat.) ± 0.026 (sys.) mag and has been adopted by Riess et al. (2019) for the Cepheid distances and by Freedman et al. (2019) for the TRGB estimates.

The statistical errors on SBF distances for all the objects listed in Table 1 are taken as reported in the corresponding papers. The uncertainties include the propagation of the errors on both the intercept and the slope of the SBF calibration reported in Eq. (1) of Tonry et al. (2001). The systematic error (not included in the SBF distance error) has been estimated including the uncertainty in the tie of the SBF distances to the Cepheid distance scale, which is conservatively evaluated to be 0.1 mag (see e.g., Freedman & Madore 2010; Cantiello et al. 2018a). This error is dominated by the uncertainty on the LMC distance (Tonry et al. 2001).

[1] https://sne.space/

Table 1. Calibration sample of SNe Ia hosted in galaxies that have SBF distance modulus measurements.

Supernova	Host galaxy	μ_{SBF} (mag)	σ_{SBF} (mag)	Morpholgy	Distance reference	$\log M_*$ ($M_\odot$)	$\sigma_{\log M_*}$ ($M_\odot$)
SN2000cx	NGC 524	31.921	0.212	SA0(rs)	Tonry et al. (2001)	10.929	0.090
SN1994D	NGC 4526	31.320	0.120	SAB0(s)	Cantiello et al. (2018b)	10.996	0.055
SN2007on	NGC 1404	31.526	0.072	E1	Blakeslee et al. (2009)	10.932	0.035
SN2012cg	NGC 4424	31.020	0.180	SB(s)a	Cantiello et al. (2018b)	9.706	0.083
SN1980N	NGC 1316	31.590	0.050	SAB0(s)pec	Cantiello et al. (2013)	11.514	0.032
SN2003hv	NGC 1201	31.566	0.304	SA0(r)	Tonry et al. (2001)	10.565	0.064
SN2008Q	NGC 524	31.921	0.212	SA0(rs)	Tonry et al. (2001)	10.929	0.090
SN1970J	NGC 7619	33.582	0.151	E	Mei et al. (2003)	11.340	0.073
SN1983G	NGC 4753	31.919	0.197	I0	Tonry et al. (2001)	11.148	0.064
SN2014bv	NGC 4386	32.190	0.494	SAB0	Tonry et al. (2001)	10.480	0.064
SN2015bp	NGC 5839	31.737	0.314	SAB0(rs)	Tonry et al. (2001)	9.979	0.137
SN2016coj	NGC 4125	31.922	0.258	E6 pec	Tonry et al. (2001)	11.083	0.064
SN1981D	NGC 1316	31.590	0.050	SAB0(s)pec	Cantiello et al. (2013)	11.514	0.032
SN1992A	NGC 1380	31.632	0.075	SA0	Blakeslee et al. (2009)	10.931	0.032
SN2018aoz	NGC 3923	31.795	0.101	E4-5	Cantiello et al. (2007)	11.204	0.065
SN2011iv	NGC 1404	31.526	0.072	E1	Blakeslee et al. (2009)	10.932	0.035
SN2006dd	NGC 1316	31.590	0.050	SAB(s)pec	Cantiello et al. (2013)	11.514	0.032
SN1992bo	E352−057	34.270	0.150	SB0(s)pec	Ajhar et al. (2001)	10.395	0.071
SN1997E	NGC 2258	33.500	0.150	SA0(r)	Ajhar et al. (2001)	11.199	0.069
SN1995D	NGC 2962	32.600	0.150	SAB0(rs)	Ajhar et al. (2001)	10.597	0.069
SN1996X	NGC 5061	32.260	0.190	E0	Ajhar et al. (2001)	11.057	0.086
SN1998bp	NGC 6495	33.100	0.150	E	Ajhar et al. (2001)	10.462	0.069
SN2017fgc	NGC 474	32.536	0.133	SA0(s)	Cantiello et al. (2007)	10.568	0.061
SN2020ue	NGC 4636	30.830	0.130	E0	Tonry et al. (2001)	10.803	0.061

Notes. The 24 SNe Ia listed here form the SBF calibration sample used in this work.

2.2. SH0ES calibration sample

In order to compare the SN distances and the H_0 estimated using the SBF calibration with those estimated from Cepheid calibration, we also take the SH0ES sample of 19 galaxies from Riess et al. (2016, 2019) as a second calibrator set. These galaxies host a SN Ia and have their distances estimated using Cepheid variable stars. Their distance moduli (and associated uncertainties) are taken from Table 5 of Riess et al. (2016, hereafter R16), and the photometric data of the SNe Ia are retrieved from the Open Supernova Catalog.

The Cepheid distances taken from R16 are calibrated using the near-infrared (NIR) and optical Cepheid P–L relations. Using only the optical relation they find $H_0 = 71.56 \pm 2.49\,\mathrm{km\,s^{-1}\,Mpc^{-1}}$, which is ∼2% smaller than the NIR-based estimate of $H_0 = 73.24 \pm 1.74\,\mathrm{km\,s^{-1}\,Mpc^{-1}}$. The optical Cepheid P–L relations used by R16 are described in Hoffmann et al. (2016), where it is also shown that their optical P–L relations are in very good agreement with the P–L relations of Udalski et al. (1999), adopted in F01. Moreover, three of the 19 SH0ES calibrators are also present in F01, namely NGC 1365, NGC 4536, and NGC 4639. For these three galaxies, the differences between the distance modulus from R16 and the metallicity corrected one from F01 are 0.04, 0.04, and −0.18 mag, respectively. Although it is not a statistically significant comparison, they show no systematic offset.

Multiple SN analyses show correlations between luminosity of the SN Ia and the host galaxy mass (e.g., Kelly et al. 2010; Lampeitl et al. 2010; Sullivan et al. 2010; Gupta et al. 2011), age, metallicity and star formation rate (SFR; e.g., Hayden et al. 2013; Rigault et al. 2013, 2015; Roman et al. 2018). Thus, the SN luminosity dependence on host galaxy properties is another important ingredient that should be taken into account for any SN studies. Differences between the properties of the host galaxies of the calibrating sample and that of the Hubble-flow sample may introduce systematic errors in the value of H_0 (see e.g., Freedman et al. 2019). Different host environments can also affect the extinction suffered by the SN luminosity, which is another issue to be addressed in SN Ia cosmology (Brout & Scolnic 2020).

The SH0ES sample is mainly composed of late-type spiral galaxies as Cepheids are relatively young stars. On the other hand, the SBF sample is biased toward early-type galaxies (92% of the SBF sample) dominated by old stellar populations. Figure 1 shows the histograms (top panel) and the density distributions (bottom panel) of the stellar mass of the host galaxies belonging to the SBF and SH0ES calibration samples. The SH0ES sample has a substantially lower mean galaxy stellar-mass (log stellar masses in units of $M_\odot$) of 9.97 than the SBF sample (10.87). We note that only one SN, namely SN2012cg hosted in NGC 4424, is common among the two calibration samples. For comparison, Fig. 1 also shows the distribution of the host-galaxy stellar masses for the cosmological sample described in the next section.

2.3. Cosmological sample

For measuring the Hubble constant, we build a statistically significant sample of SNe Ia extending into the Hubble flow. We extract our cosmological sample from the Combined Pantheon Sample (Scolnic et al. 2018), which consists of 1048 spectroscopically confirmed SNe Ia coming from various local and high-redshift supernova surveys. All the SNe are

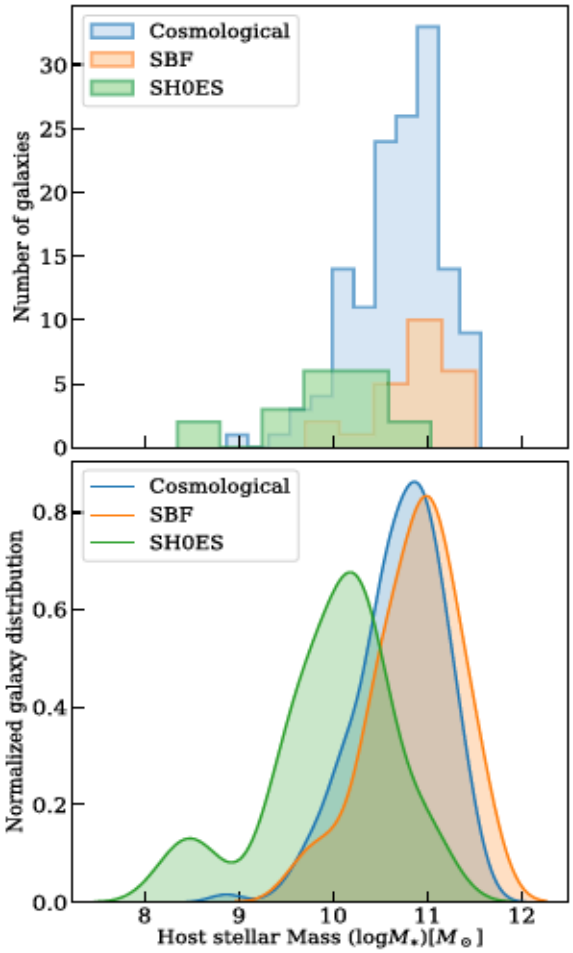

Fig. 1. Number of galaxies (*top panel*) and the normalized density distribution (*bottom panel*) as a function of the host galaxy stellar mass for the SBF and the SH0ES calibration samples. We also plot the host stellar mass distribution for the cosmological sample. The KS-test P value for the two calibration samples gives 6.03×10^{-6}, indicating that the stellar mass distributions of the host galaxies of SNe Ia are different for the two samples.

cross-calibrated with the Pan-STARRS (PS1) survey in order to have a common photometric calibration (Scolnic et al. 2015). We select all the SNe Ia spanning a redshift range of $0.009 < z < 0.075$, with good quality photometric data to appropriately sample the LC, and with 2MASS K_s-band magnitude to evaluate the galaxy stellar-mass. We also exclude fast decliners and very red SNe Ia from the sample (as described in Sect. 3). This gives us a sample of 140 SNe Ia, referred to as the full cosmological sample hereafter.

The main contributions to the data sample come from the Harvard Smithsonian Center for Astrophysics CfA1-CfA4 (Riess et al. 1999; Jha et al. 2006; Hicken et al. 2009a,b, 2012) and the Carnegie Supernova Project (CSP, Contreras et al. 2010; Folatelli et al. 2010; Stritzinger et al. 2011) survey. The optical photometric data of the SNe of the cosmological sample are assembled using data stored in a dedicated repository[2], and are analyzed in the same way as the data of the SNe Ia belonging to the calibration samples.

Since the lower redshift range of this cosmological sample starts with $z = 0.009$, where peculiar velocities can have a significant impact on the recessional velocities of the galaxies, we apply a more stringent redshift cut removing all galaxies below $z = 0.02$ (similar to R16) in order to mitigate the contamination from peculiar velocities. This sample cut leaves 96 SNe in the cosmological set and is referred to as the redshift-cut cosmological sample throughout this work. Our main results will be based on the use of the redshift-cut cosmological sample, although we will also estimate H_0 using the full cosmological sample for comparison with studies such as Freedman et al. (2019).

To summarize, this work has two calibration sets: the SBF sample, which is our main sample consisting of 24 SNe Ia, and the SH0ES sample from R16 that has 19 SNe Ia. The calibrations derived from these two are applied to the full cosmological sample consisting of 140 SNe Ia and its subsample of 96 SNe Ia with the redshift cut.

3. Analysis

While the exact nature of SN Ia progenitors remains uncertain, the regularity of their observed properties enables us to use them for measuring precise distances. This relies on the empirical evidence that their intrinsic luminosity is correlated with the rate of decline of their light curves and hence they can be standardized (Phillips 1993; Riess et al. 1996; Perlmutter et al. 1997). Considering this and further implementing correction terms that take into account the absolute luminosity dependence on the color and the host galaxy, SNe Ia can be used as standard candles for cosmological studies.

3.1. Lightcurve fitting

In order to evaluate the SN luminosity from the observable LC properties, we fit the LCs of all the SNe Ia in this study belonging to the two calibration samples and the cosmological sample. We estimate their apparent magnitudes at maximum in the B and V bands, along with the LC shape. For this, we use the `SNooPy` (SuperNovae in Object Oriented Python) LC fitter (Burns et al. 2011). `SNooPy` corrects the photometry data for Milky Way extinction using the dust maps of Schlafly & Finkbeiner (2011), and applies the K-corrections that are computed using the SED template sequence developed by Hsiao et al. (2007). We fit the LC using the "max-model" method[3], which gives us the epoch and the magnitude (for each filter) of the LC maximum, and the LC shape parameter s_{BV}, called the "color-stretch" parameter (Burns et al. 2014). For five SNe Ia in our calibration sample, pre-maximum LC observations are missing. However while fitting the LCs using SN templates, `SNooPy` is able to reproduce the LC shape at epochs where there are no data as described in Burns et al. (2011). Provided that the peak is well sampled, it ensures reliable modeling of the SNe without pre-max data.

The color-stretch parameter takes into account the color ($m_B - m_V$) evolution of the SNe Ia and is calculated by getting the time between B maximum and ($m_B - m_V$) maximum (the typical value for which is 30 days) and dividing this time by 30. Here, $m_B - m_V$ refers to real color evolution of the SNe Ia, and it is different from the pseudo-color mentioned before. We use s_{BV} as the LC shape parameter, instead of the more commonly used Δm_{15} (magnitude decline between the LC maximum and 15 days later) because s_{BV} properly captures the behavior of fast decliners and it is appropriately sensitive to the extinction (Burns et al. 2014, 2018). For "normal" SNe Ia s_{BV} is about 1, while for fast

[2] http://snana.uchicago.edu/downloads.php

[3] For details see the online documentation of SNooPy: https://csp.obs.carnegiescience.edu/data/snpy/documentation

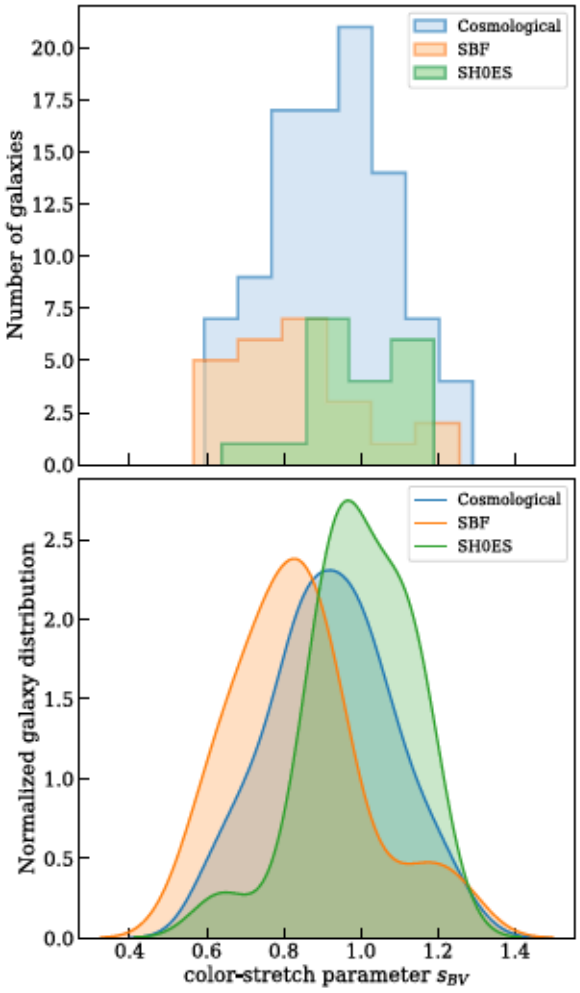

Fig. 2. Number of galaxies (*top panel*) and the normalized density distribution (*bottom panel*) of the s_{BV} parameter values of SNe Ia of the three data samples used in this work: the SBF calibration sample, the SH0ES calibration samples, and the cosmological sample.

decliners s_{BV} is typically smaller than 0.5. We exclude from our fiducial calibration sample fast decliner SNe Ia ($s_{BV} < 0.5$) and highly reddened SNe Ia (pseudo-color $m_B - m_V > 0.3$ mag). Figure 2 shows the histograms (top panel) and the density distributions (bottom panel) of the s_{BV} values of the SNe Ia belonging to the two calibration samples. The two calibration samples show a different distribution of s_{BV} values while the cosmological sample s_{BV} distribution lies between the two. The calibration sample contains two "transitional" objects, namely SN 2007on and SN 2011iv both located in NGC 1404, characterised by peak magnitudes similar to normal SNe Ia but with a relatively faster rate of decline (Gall et al. 2018). Since the use of the color-stretch parameterization in their LC fitting should ensure reliable modeling of their evolution, we include them in our fiducial calibration sample maintaining the threshold $s_{BV} > 0.5$ as done in previous works, such as Freedman et al. (2019) and Burns et al. (2018). However, we also perform the analysis excluding them from the sample to investigate their influence on the final results (see Sect. 4).

Table 2 lists the LC parameters for the SBF calibration sample: the maximum brightness in B and V bands along with the errors (Cols. 2–5), the s_{BV} parameter and relative error (Cols. 6 and 7), the color ($m_B - m_V$) at maximum (Col. 8) and the absolute magnitude in B band (M_B) calculated as $m_B - \mu_{SBF}$ (Col. 9), where μ_{SBF} is taken from Table 1. The B-band light curve fits of the SNe in the SBF sample are shown in Table A.1. We analyze the LCs of the SNe of the SH0ES calibration sample in the same way. The estimated LC parameters of the SH0ES SNe are given in Table 3. The LC parameters of SNe in the cosmological sample are also obtained following the same fitting analysis.

3.2. Luminosity calibration

Having obtained the light curve parameters, we proceed to derive the SN Ia calibration relation separately for the SBF and the SH0ES samples. Phillips (1993) gave the relation between Ia luminosity and their LC shape, and later Tripp (1998) added the color correction. We use this two-parameter luminosity relation, including a term relating the peak luminosity of the SN Ia to the LC shape (represented by the color-stretch parameter), and a second term for the color correction accounting for the dust reddening in the host galaxy. The apparent B band peak magnitude (m_B) of a SNe Ia is thus modeled as:

$$m_B = P^N(s_{BV} - 1) + R(m_B - m_V) + \mu_{\rm calib}, \quad (1)$$

where P^N is a polynomial of order N as a function of $(s_{BV} - 1)$, which gives the luminosity-decline rate relation, R is the extinction correction coefficient that correlates the peak magnitude with the color ($m_B - m_V$) at maximum, and $\mu_{\rm calib}$ is the distance modulus for the host galaxy (μ_{SBF} taken from Table 1 for the SBF sample, and $\mu_{\rm ceph}$ taken from Table 5 of R16 for the SH0ES sample).

Besides the Milky Way extinction correction (already included in the LC fitting procedure as described in Sect. 3.1), there are three other potential sources of reddening that need to be corrected for: (1) intergalactic dust, (2) interstellar dust of the host galaxy, and (3) the intrinsic color of SNe Ia (Burns et al. 2014; Foley & Kasen 2011; Maeda et al. 2011). To know the properties of these different sources, which may vary from SN to SN, and then disentangle their different effects requires sophisticated color modeling (see, e.g., Burns et al. 2014). Since cosmological analyses do not aim at studying the details of dust properties, we make no distinction between the intrinsic and the extrinsic sources of color variation, and combine the extinction from these different effects into the one correlation term R, as done by previous works such as Betoule et al. (2014), Freedman et al. (2009), and Conley et al. (2011).

In order to identify the optimum model for our SBF calibrators data, we first perform the analysis using the quadratic polynomial ($N = 2$) and then with only the linear polynomial ($N = 1$) in P. The comparison of the luminosity-stretch (s_{BV}) relation obtained by the two model forms shows that the second-order term does not improve the fits. The R^2 score (coefficient of determination[4]) of both the fits was calculated to be 0.96 and mean squared error (MSE) as 0.06. The value of P^2 parameter was estimated to be 0.35 ± 1.33, which makes it consistent with zero and hence its weight in the model is null. Therefore, we use the calibration relation with the linear term in P^N:

$$m_B = P^0 + P^1(s_{BV} - 1) + R(m_B - m_V) + \mu_{\rm calib}, \quad (2)$$

[4] The R^2 score is defined as $(1 - u/v)$, where u is the residual sum of squares $\sum (y_{\rm true} - y_{\rm pred})^2$ and v is the total sum of squares $\sum (y_{\rm true} - \overline{y_{\rm true}})^2$.

Table 2. Best-fit lightcurve parameters of the SNe Ia of the SBF sample estimated using SNooPy.

Supernova	m_B (mag)	σ_{m_B} (mag)	m_V (mag)	σ_{m_V} (mag)	s_{BV}	$\sigma_{s_{BV}}$	m_B-m_V (mag)	M_B (mag)
SN2000cx	13.134	0.007	13.069	0.006	0.907	0.006	0.065	−18.788
SN1994D	11.769	0.007	11.827	0.005	0.784	0.006	−0.058	−19.551
SN2007on	13.046	0.004	12.931	0.004	0.566	0.005	0.114	−18.480
SN2012cg	12.116	0.008	11.930	0.008	1.101	0.019	0.186	−18.904
SN1980N	12.459	0.011	12.334	0.012	0.848	0.011	0.125	−19.131
SN2003hv	12.455	0.049	12.544	0.036	0.764	0.020	−0.089	−19.111
SN2008Q	13.459	0.014	13.512	0.010	0.804	0.022	−0.053	−18.463
SN1970J	14.865	0.037	14.619	0.037	0.916	0.029	0.246	−18.717
SN1983G	12.789	0.102	12.614	0.071	1.189	0.059	0.175	−19.131
SN2014bv	13.999	0.018	13.809	0.013	0.640	0.021	0.190	−18.191
SN2015bp	13.697	0.014	13.664	0.016	0.681	0.018	0.033	−18.040
SN2016coj	13.205	0.021	12.978	0.013	0.891	0.011	0.227	−18.717
SN1981D	12.486	0.048	12.327	0.046	0.852	0.041	0.159	−19.104
SN1992A	12.530	0.004	12.500	0.004	0.777	0.006	0.030	−19.102
SN2018aoz	12.515	0.009	12.590	0.008	0.841	0.007	−0.075	−19.280
SN2011iv	12.446	0.008	12.389	0.009	0.652	0.014	0.057	−19.080
SN2006dd	12.270	0.003	12.287	0.003	0.950	0.003	−0.017	−19.320
SN1992bo	15.758	0.013	15.746	0.011	0.712	0.013	0.011	−18.512
SN1997E	15.171	0.009	15.082	0.007	0.795	0.012	0.090	−18.329
SN1995D	13.379	0.033	13.253	0.015	1.256	0.025	0.126	−19.221
SN1996X	13.075	0.024	13.081	0.017	0.893	0.022	−0.006	−19.185
SN1998bp	15.368	0.013	15.071	0.014	0.597	0.025	0.297	−17.732
SN2017fgc	13.619	0.019	13.345	0.014	0.957	0.018	0.273	−18.917
SN2020ue	11.970	0.011	12.071	0.008	0.718	0.012	0.101	−18.860

Notes. m_B and m_V (Cols. 2 and 4) are the apparent magnitudes at maximum in the B and V bands, and s_{BV} (Col. 6) is the stretch color parameter (Col. 7). The color m_B-m_V (Col. 8) is computed as the difference between the maximum brightness in B and V bands, and M_B (Col. 9) is the absolute magnitude in B band, computed as $m_B-\mu_{\rm SBF}$, where $\mu_{\rm SBF}$ is taken from Table 1.

Table 3. Best-fit parameters of the SH0ES sample estimated using SNooPy.

Supernova	m_B (mag)	σ_{m_B} (mag)	m_V (mag)	σ_{m_V} (mag)	s_{BV}	$\sigma_{s_{BV}}$	m_B-m_V (mag)	M_B (mag)
SN1995al	13.339	0.010	13.172	0.010	1.075	0.018	0.167	−19.159
SN2011by	12.889	0.009	12.821	0.009	0.947	0.007	0.068	−18.698
SN2012fr	11.976	0.006	11.943	0.004	1.122	0.009	0.033	−19.331
SN1981B	11.863	0.016	11.788	0.021	0.639	0.038	0.075	−19.043
SN2003du	13.492	0.004	13.548	0.004	1.011	0.004	−0.056	−19.427
SN2005cf	13.250	0.004	13.246	0.004	0.947	0.004	0.004	−19.013
SN2011fe	9.930	0.004	9.947	0.003	0.937	0.003	−0.017	−19.205
SN2013dy	12.757	0.004	12.554	0.003	1.136	0.010	0.203	−18.742
SN2002fk	13.205	0.023	13.209	0.017	1.189	0.034	−0.004	−19.318
SN1998aq	12.322	0.006	12.414	0.004	0.940	0.004	−0.092	−19.415
SN2007af	13.164	0.003	13.058	0.003	0.919	0.003	0.106	−18.622
SN1994ae	13.064	0.051	12.933	0.041	1.125	0.157	0.131	−19.008
SN2012cg	12.116	0.008	11.930	0.008	1.101	0.019	0.186	−18.964
SN2015F	12.823	0.009	12.695	0.010	0.865	0.007	0.128	−18.688
SN1990N	12.650	0.008	12.574	0.006	0.976	0.006	0.076	−18.882
SN2007sr	12.741	0.058	12.568	0.042	1.022	0.023	0.173	−18.549
SN2012ht	12.393	0.004	12.576	0.005	0.854	0.004	−0.183	−19.515
SN2009ig	13.478	0.008	13.372	0.007	1.134	0.023	0.106	−19.019
SN2001el	12.831	0.007	12.601	0.005	0.949	0.006	0.230	−18.480

Notes. m_B and m_V (Cols. 2 and 4) are the apparent magnitudes at the light curve maximum in the B and V bands, respectively. s_{BV} (Col. 6) is the stretch color parameter (Col. 7). The color is given as m_B-m_V is computed as difference between the maximum brightness in B and V bands and M_B (Col. 9) is the absolute magnitude in B band, computed as $m_B-\mu_{\rm ceph}$, where $\mu_{\rm ceph}$ is taken from Table 5 of R16.

3.3. The Hubble constant

In order to estimate H_0, we use a purely kinematic cosmological model that gives the luminosity distance as a function of redshift (Weinberg 1972; Visser 2004). The parametrization assumes a Robertson–Walker metric in a flat space for the geometry of the Universe and it is based on the Taylor series expansion of the Hubble–Lemaitre law, with the presence of two additional parameters, q_0 and j_0, where $q_0 = -\ddot{a}a^{-2}a$ is the cosmic deceleration and $j_0 = -\dddot{a}a^{-3}a^2$ is the third derivative of the scale factor, called cosmic jerk. For a flat Universe, the expansion of the luminosity distance to the third order in z is given as:

$$d_{\rm L}(z) = \frac{cz}{H_0}\left\{1+\frac{1}{2}(1-q_0)z-\frac{1}{6}(1-q_0-3q_0^2+j_0)z^2+O(z^3)\right\}. \quad (3)$$

Neglecting $O(z^3)$ and higher order term, the corresponding distance modulus is given as

$$\mu(z,\, H_0) = 5\log_{10}\frac{cz}{H_0}\left\{1+\frac{1}{2}(1-q_0)z-\frac{1}{6}(1-q_0-3q_0^2+j_0)z^2\right\}+25. \quad (4)$$

For the cosmological sample, we use Eq. (2) except that the independent distance moduli $\mu_{\rm calib}$ are replaced with distance moduli as a function of H_0 and the redshift as given by Eq. (4). H_0 is left as a free parameter in the analysis. Hence the intercept term P^0 is anchored only to the independent distances of the calibration sample, and it dictates the uncertainty in the estimated Hubble constant value. We fix the value of the deceleration parameter to $q_0 = -0.55$ and the jerk $j_0 = 1$ (Planck Collaboration VI 2020; Betoule et al. 2014). In the redshift range of our cosmological sample ($0.009 < z < 0.075$), any assumption about the expansion history of the Universe does not significantly affect the final estimate of H_0 (Dhawan et al. 2020). Hence, fixing the values of q_0 and j_0 does not bias our H_0 estimates.

3.4. Bayesian inference

We perform a hierarchical Bayesian regression using the data of both the calibration sample and the cosmological sample to estimate the free model parameters using Markov chain Monte Carlo (MCMC) sampling. The modeling here combines two submodels, one for the calibration sample and one for the cosmological sample, and estimates the posterior distributions for the parameters of interest from both the SN Ia populations simultaneously. Bayes' theorem gives the posterior of the model parameters as

$$P(\Theta|D) \propto P(D|\Theta)P(\Theta), \quad (5)$$

where D denotes the vector for the observed SN data (the LC fit parameters: m_B, m_V, s_{BV}), and Θ denotes the vector for the model parameters, namely P^0, P^1, R, and H_0. Each individual SN can be assumed to have its own model parameters Θ_i (i.e., P_i^0, P_i^1, R_i) but they cannot be sufficiently constrained on a SN-by-SN basis and their uncertainties propagate to the H_0 inference on the population level. This makes it necessary that the model assumptions and priors for each SN are propagated hierarchically when inferring the parameters from a population of SNe. Hence, the distribution of each Θ_i is assumed to be Gaussian with a mean of Θ making it the hyper-parameter vector. Then the hyper-parameters P^0, P^1, and R describe the distribution (Gaussian width) of the model parameters of each individual supernova and their priors are the hyper-priors of the model.

Then, marginalising over all Θ_i, the likelihood probability distribution $P(D|\Theta)$ is given as the combined distribution for the calibrator and cosmological SNe,

$$P(D|\Theta) = \prod_{i=1}^{N_{\rm calib}} P(D_i, \mu_{{\rm calib},i}|\Theta) \prod_{j=1}^{N_{\rm cosmo}} P(D_j, z_j|\Theta, H_0), \quad (6)$$

where i is the index for the $N_{\rm calib}$ SNe of the calibration sample (24 for SBF and 19 for SH0ES) and j for the $N_{\rm cosmo}$ SNe of the cosmological sample. $\mu_{{\rm calib},i}$ are the independent distance estimates of the calibrating set and $D_{i/j}$ is the data set on an individual SN of the calibrator (i) or the cosmological sample (j). P^0, P^1, R, and H_0 are kept as free parameters and are determined simultaneously. The redshift z_j of each SN belonging to the cosmological sample is in the CMB rest frame, and is taken from the online repository as described in Sect. 2.3. Assuming normally distributed errors and treating the B band peak magnitude as the target variable, the log likelihoods for the two samples can be written as

$$\ln \mathcal{L}_{\rm calib} = -\frac{1}{2}\sum_{i=1}^{N_{\rm calib}} \frac{(m_B^i - m_B^{\rm T})^2}{\sigma^2_{{\rm calib},i}} - \frac{1}{2}\sum_{i=1}^{N_{\rm calib}} \ln 2\pi\sigma^2_{{\rm calib},i} \quad (7)$$

and

$$\ln \mathcal{L}_{\rm cosmo} = -\frac{1}{2}\sum_{j=1}^{N_{\rm cosmo}} \frac{(m_B^j - m_B^{\rm T})^2}{\sigma^2_{{\rm cosmo},j}} - \frac{1}{2}\sum_{i=j}^{N_{\rm cosmo}} \ln 2\pi\sigma^2_{{\rm cosmo},j}, \quad (8)$$

while the combined log likelihood is

$$\ln \mathcal{L} = \ln \mathcal{L}_{\rm calib} + \ln \mathcal{L}_{\rm cosmo}. \quad (9)$$

Here, $m_B^{i/j}$ is the observed B band magnitude for each supernova, and $m_B^{\rm T}$ is the true magnitude given by Eq. (2) for the calibration sample (and replacing $\mu_{\rm calib}$ with $\mu(z,\, H_0)$ in that equation for the cosmological sample). The variances $\sigma_{\rm calib/cosmo}$ are computed as quadrature sum of the photometric errors and the SBF distance uncertainties. Additionally, in order to account for hidden systematic uncertainties, we include two separate intrinsic scatter parameters, one each for the two samples. These two terms, namely $\sigma_{\rm int,calib}$ and $\sigma_{\rm int,cosmo}$, are added to the variance of their respective sample and are left as free parameters in the analysis accounting for any extra dispersion observed in the measured distance moduli. It should be noted here that we do not include the correlations between light curve fit parameters since they are negligible, while correlations between model parameters are taken into account in the analysis. Hence, the full variance for a given calibrator object i is

$$\sigma^2_{{\rm calib},i} = \sigma^2_{m_B,i} + \sigma^2_{\mu_{{\rm SBF},i}} + (P^1\sigma_{s_{BV},i})^2 + (R\sigma_{m_B-m_V,i})^2 - 2R\sigma^2_{m_B,i} + \sigma^2_{\rm int,calib}, \quad (10)$$

and the total variance for an object j in cosmological sample is

$$\sigma^2_{{\rm cosmo},j} = \sigma^2_{m_B,j} + (P^1\sigma_{s_{BV},j})^2 + (R\sigma_{m_B-m_V,j})^2 - 2R\sigma^2_{m_B,j} + \sigma^2_{\rm int,cosmo}. \quad (11)$$

Lastly, the term $P(\Theta)$ in Eq. (5) are the priors on our model parameters. We adopt uniform priors for all the parameters except the intrinsic scatter terms for which we assume a Half Cauchy distribution. The MCMC sampling is implemented using the "No U-Turn Sampler" (NUTS) provided in the `PyMC3`[5]

[5] See https://docs.pymc.io/

Table 4. Mean posterior values for the luminosity correlation parameters and associated errors for the full cosmological sample and the redshift-cut sample.

Redshift range	$N_{\rm sample}$ (mag)	P_0 (mag)	P_1 (mag)	R	$\sigma_{\rm int,calib}$ (mag)	$\sigma_{\rm int,cosmo}$ (mag)
SBF calibration						
$0.009 < z < 0.075$	140	-19.23 ± 0.07	-1.07 ± 0.11	2.03 ± 0.16	0.29	0.18
$0.02 < z < 0.075$	96	-19.22 ± 0.07	-1.05 ± 0.12	2.01 ± 0.17	0.29	0.15
Cepheid calibration						
$0.009 < z < 0.075$	140	-19.16 ± 0.05	-1.00 ± 0.11	2.15 ± 0.16	0.17	0.18
$0.02 < z < 0.075$	96	-19.16 ± 0.05	-0.99 ± 0.12	2.16 ± 0.17	0.17	0.15

Notes. The last two columns on the right give the intrinsic scatter of the calibration sample and the cosmological samples. The top part of the table shows the results obtained using the SBF calibration sample, and the bottom part the results obtained using the SH0ES calibration sample.

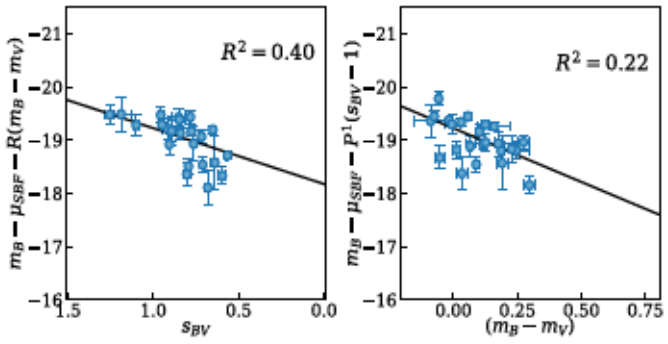

Fig. 3. Luminosity correlation plots for the SBF sample: the absolute magnitude ($m_B - \mu_{\rm SBF}$) corrected for the color vs. the LC stretch parameter (*left panel*), and the absolute magnitude corrected for the LC stretch vs. color (*right panel*). The correlation parameters are evaluated using the Bayesian analysis described in Sect. 3.4. The solid black lines show the best-fit model obtained with the MCMC sampling. The R^2 score (coefficient of determination) of the fit is shown in the top right.

(Salvatier et al. 2016), which is a `python` probabilistic programming package. Using the observed data as input, we estimate simultaneously the posteriors for the correlation parameters P^0, P^1, R and the Hubble constant H_0 along with the two intrinsic scatters. All the best-fit values provided in this work are the posterior means and the errors in the parameters are the standard deviation of their posterior. The entire data sets for the three samples and the full analysis codes used in this paper are available in a GitHub repository[6].

4. Results

4.1. SBF calibration

Using the SBF calibration sample of 24 SNe Ia and the redshift-cut cosmological sample of 96 SNe Ia ($z > 0.02$), we evaluate the posterior distributions of the luminosity correlation parameters and the Hubble constant. The analysis is also performed on the full cosmological sample of 140 SNe Ia. Table 4 gives the mean posterior values for the correlation parameters and the individual intrinsic scatter for both the SBF calibration sample and the cosmological samples. Figure 3 shows the luminosity relations for the SBF calibration sample with respect to the stretch parameter (left panel) and the color (right panel).

The best-fit value of the Hubble constant obtained using the SBF calibration on the redshift-cut cosmological sample is $H_0 = 70.50 \pm 2.37\,{\rm km\,s^{-1}\,Mpc^{-1}}$. It is slightly lower, $H_0 = 69.18 \pm 2.33\,{\rm km\,s^{-1}\,Mpc^{-1}}$ when the full cosmological sample is used. The computed H_0 values are listed in Table 5. A corner plot showing posterior samples for SBF calibration is given in Fig. 4.

In order to investigate the influence of the adopted threshold of the s_{BV} parameter ($s_{BV} > 0.5$) on our results, we evaluate the H_0 removing the two transitional objects SN2007on and SN2011iv (see Sect. 3) from our SBF calibration sample. The net effect is a small increase of 0.7% in H_0. Furthermore, assuming a more conservative definition of fast decliners in the SBF calibration sample by removing all SNe with $s_{BV} < 0.7$ (5 SNe Ia including the two above transitional SNe Ia), the resultant H_0 value is lower by 1.8%.

4.2. Cepheid Calibration

For the Cepheid calibration, we used the SH0ES sample as calibration set and estimated the correlation parameters and the Hubble constant value following the same analysis as used for the SBF calibration. The estimated parameter values are listed in the lower part of the Table 4. It is worth noting the difference between the P_0 values for the SBF and Cepheid calibration and the slightly higher R value for the SH0ES calibration. The luminosity relations for the SH0ES calibration sample are shown in Fig. 5.

Applying the SH0ES Cepheid calibration to the redshift-cut cosmological sample, the mean value for H_0 is found to be $H_0 = 72.84 \pm 1.66\,{\rm km\,s^{-1}\,Mpc^{-1}}$, and it decreases to $H_0 = 71.51 \pm 1.66\,{\rm km\,s^{-1}\,Mpc^{-1}}$ when using the full cosmological sample. These values are listed in Table 5. The value of the Hubble constant evaluated for the redshift-cut cosmological sample is fully consistent with the measurement of R16 ($H_0 = 73.24 \pm 1.74$). The posterior samples for the SH0ES calibration analysis are given in Fig. 6.

For fitting the SN Ia LCs, we prefer to use `SNooPy` instead of SALT2 (Mosher et al. 2014) since the latter has not been trained on fast-declining SNe, this results in poorly constrained LC shape parameter (x_1) for faster SNe Ia, as shown in Fig. 1 of Burns et al. (2018). Our SBF calibration sample contains 11 of 26 SNe with $0.5 < s_{BV} < 0.8$, motivating our choice for using SNooPy. The fact that the H_0 value obtained with the SH0ES calibration is in perfect agreement with R16 confirms that using `SNooPy` instead of SALT2 (as used by R16) provides consistent results.

In order to make the SBF and SH0ES calibration samples completely independent, we performed the analysis removing the one object in common between the SBF and SH0ES samples,

[6] https://github.com/nanditakhetan/SBF_SNeIa_H0

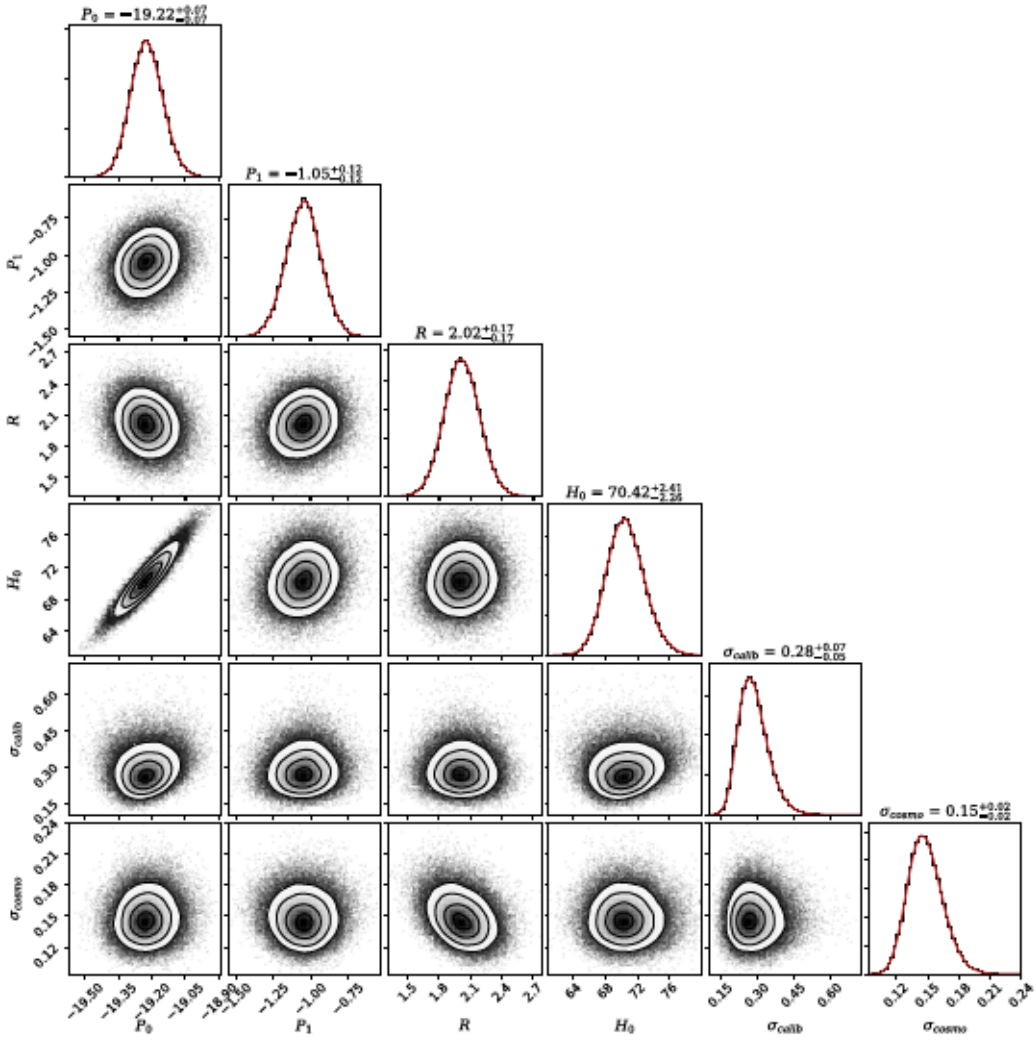

Fig. 4. Corner plot showing posterior distributions for the parameters P_0, P_1, R, and H_0 along with the intrinsic scatter obtained using the SBF sample (24 SNe Ia) with the redshift-cut cosmological sample (96 SNe Ia). The title on each histogram shows the median value of the respective posterior distribution. The luminosity correction does not include any dependence on host galaxy stellar mass.

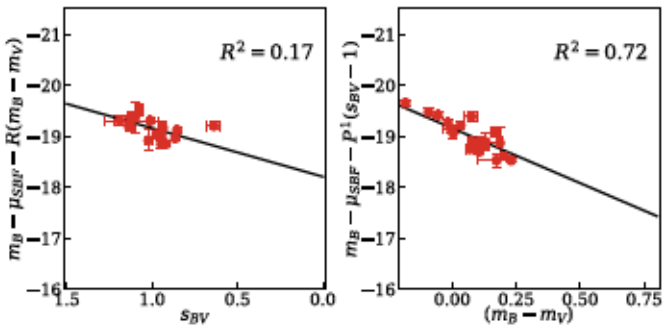

Fig. 5. Luminosity correlation parameters for the SH0ES sample: the absolute magnitude ($m_B - \mu_{SBF}$) corrected for the color vs. the LC stretch parameter (*left panel*), the absolute magnitude corrected for the LC stretch vs. color (*right panel*). The correlation parameters are evaluated using the Bayesian analysis. The solid black lines show the best-fit model obtained with the MCMC sampling. The R^2 score (coefficient of determination) of the fit is shown in the top right.

SN2012cg. The H_0 results from both the SBF and SH0ES calibrations remain the same.

Table 5. H_0 values for the full cosmological sample and the redshift-cut cosmological sample that is obtained excluding the SNe Ia with $z < 0.02$.

Sample cut	SBF calibration		Cepheid calibration	
	H_0	σ_{H_0}	H_0	σ_{H_0}
$0.009 < z < 0.075$	69.18	2.33	71.51	1.66
$0.02 < z < 0.075$	70.50	2.37	72.84	1.66

Notes. The H_0 values are given for both the SBF (central column) and the Cepheid (right column) calibrations.

As noted in Sect. 2.1, the SBF distances of our calibration sample are based on the LMC distance modulus of 18.50 ± 0.10 mag, as in F01, and the SH0ES sample distances are based on the LMC distance modulus of 18.493±0.008 mag R16. Referring to the most recent estimate of LMC distance, which is 18.477 ± 0.004 by Pietrzyński et al. (2019), we evaluated the H_0 by scaling down the SBF distances and the SH0ES distances by 0.023 mag and 0.016 mag, respectively. Using this recent value of LMC distance, the H_0 value calibrated with SBF increases by

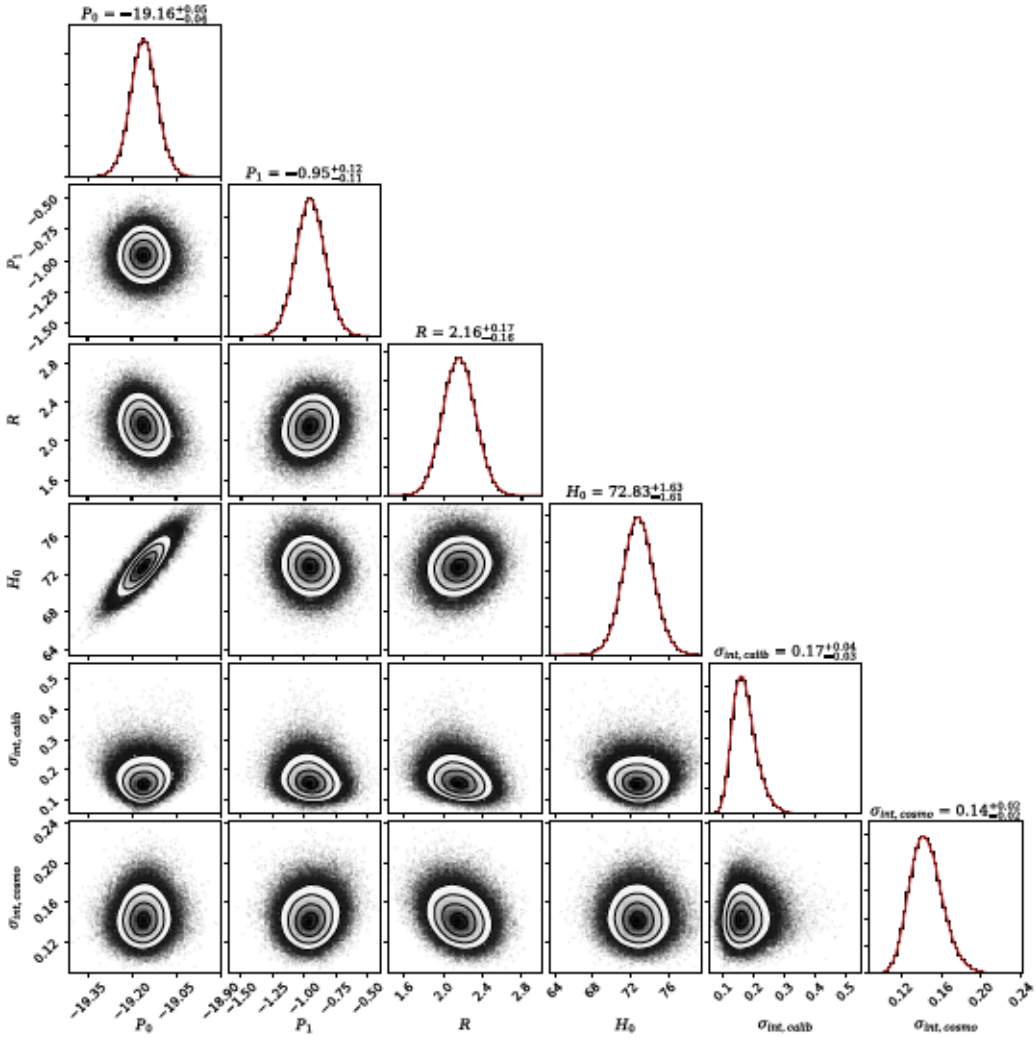

Fig. 6. Corner plot showing posterior distributions for the parameters P_0, P_1, R, and H_0 along with the intrinsic scatter obtained using the SH0ES sample with the redshift-cut cosmological sample. The title on each histogram shows the median value of the respective posterior distribution. The luminosity correction does not include any dependence on host galaxy stellar mass.

1%, becoming $71.16 \pm 2.38\,\mathrm{km\,s^{-1}\,Mpc^{-1}}$. The H_0 value calibrated with the SH0ES calibration increases by 0.8%, becoming $73.38 \pm 1.66\,\mathrm{km\,s^{-1}\,Mpc^{-1}}$. However, a truly updated revision of the SBF calibration, errors, and, hence, distances, would require a comprehensive update of Cepheid distances (P–L relations and zero-point) and the SBF measurement for the six Cepheid-host calibrating sample, which goes beyond the scope of this paper.

Figure 7 shows the Hubble diagram for the cosmological samples plotting the distance moduli versus the redshift. The plotted distance moduli are computed using the luminosity calibration relation obtained with the SBF sample. The solid line shows the best-fit model derived from the Bayesian regression. Residuals from the best-fit are shown in the bottom panel.

4.3. H_0 systematic uncertainties

The systematic uncertainty on H_0 is calculated by combining in quadrature the systematic error on SBF measurements and those from the SN LC fitting estimated by `SNooPy`. The adopted systematic errors are shown in Table 6. Our final H_0 value and its uncertainties, obtained using the SBF calibration (24 SNe Ia, without including any host galaxy dependence), is $H_0 = 70.50 \pm 2.37\,(\pm 3.4\%\ \mathrm{stat.}) \pm 3.38\,(\pm 4.8\%\ \mathrm{sys.})\,\mathrm{km\,s^{-1}\,Mpc^{-1}}$.

Deriving the Hubble constant using SBF is a five step approach, which starts with a geometric distance (e.g., LMC), followed by calibration of the Cepheid period–luminosity relation, calibration of the absolute SBF magnitude by tying it to distances based on Cepheids (from the HST Key project), calibration of the SN Ia absolute magnitude (using the SNe listed in Table 1), and finally ending with the determination of the H_0. In this five step approach, the largest source of systematic uncertainty comes from tying the SBF distance scale to the Cepheid zero point (4.6%), estimated to be 0.1 mag. This uncertainty can be reduced with a recalibration of the Cepheid period–luminosity–metallicity (or color) relationships and the LMC zeropoint using *Gaia* parallaxes (Cantiello et al. 2018b). This could halve the systematic error. Another possibility is to use the theoretical calibration of $\overline{M}$, which makes SBF an independent primary calibrator for the distance ladder approach. The systematic error in H_0 estimated using SBF SNe as calibrators has room for improvement.

The last three terms reported in Table 6 are the systematic errors in the three LC fit parameters evaluated by `SNooPy`. These errors are insensitive to the quantity and quality of the LC data. They arise from the use of templates for LC fitting, which do not perfectly represent the observed data. They are evaluated as

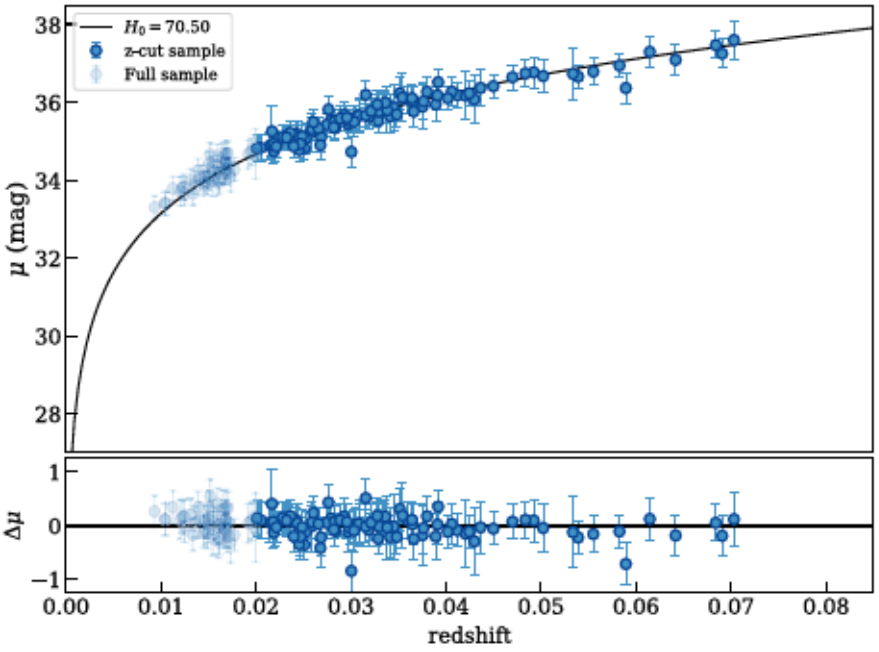

Fig. 7. Hubble diagram for the cosmological samples. The distance moduli of the SNe Ia are computed using the SBF calibration. The solid black line in the *top panel* corresponds to the H_0 value estimated for the redshift-cut cosmological sample of the 96 SNe Ia with $z > 0.02$. *Lower panel*: residual plot.

Table 6. Adopted systematic uncertainties on H_0.

Uncertainty	Magnitude	% error
SBF tie to Cepheid ZP	0.1 mag	4.6%
B-band fit	0.012 mag	0.55%
V-band fit	0.019 mag	0.87%
s_BV estimate	0.03 mag	1.4%
Total	0.106 mag	4.8%

rms in the difference between the true and template-fit values averaged over the training set.

5. Host type dependence

Considering the observational evidence that SN Ia luminosity correlates with the host galaxy type and its properties (Hamuy et al. 1996; Howell 2001; Neill et al. 2009; Pruzhinskaya et al. 2020; Ponder et al. 2020), an additional term is typically added to the luminosity correction formula (see e.g., Betoule et al. 2014; Rigault et al. 2015; Riess et al. 2016; Freedman et al. 2019), which takes into account the host galaxy stellar mass $M_\star$. This stellar-mass term is considered a proxy of other galaxy properties such as the SFR, metallicity, and/or stellar population (Sullivan et al. 2010; Kelly et al. 2010), possibly associated with different local environment and/or progenitors of the SNe.

We explore here the effect of adding the mass-based correction term (hereafter HM) to the luminosity relation of Eq. (2) and evaluate its influence on the H_0 estimate. We adopt two recipes for the mass correction: (1) a linear correction and (2) a step correction. The luminosity relation including the HM term is

$$m_B = P^0 + P^1(s_{BV} - 1) + R(m_B - m_V) + \mathrm{HM} + \mu_{\mathrm{calib}}, \quad (12)$$

where the two recipes of HM can be written as,

$$\text{Step correction: HM} = \begin{cases} \alpha_{\mathrm{step}}, & \text{for } \log_{10} M_\star/M_\odot < M_{\mathrm{step}} \\ 0, & \text{otherwise} \end{cases} \quad (13)$$

$$\text{Linear correction: HM} = \alpha_{\mathrm{linear}}(\log_{10} M_\star/M_\odot - M_0). \quad (14)$$

The step correction adds a value α_{step} to the SN absolute magnitude for all host galaxies with stellar masses below an arbitrary value M_{step} and a zero correction above it. The linear correction assumes a linear correlation of the luminosity with the host galaxy stellar mass, $\log_{10} M_\star$, given in units of solar mass, $M_\odot$, and M_0 is again an arbitrary mass zero-point. Details regarding the estimate of the host galaxy stellar mass are given in Appendix B.

We add each of the two HM corrections to the calibration relation as in Eq. (12) and perform the Hierarchical Bayesian analysis described in Sect. 3.4 using the redshift-cut cosmological sample along with the SBF and SH0ES calibration sets one by one. In order to see any possible effect of our arbitrary choices of the mass zero-point (M_0) and step mass values (M_{step}), we test it by varying these two quantities between 9 and 11.5 in steps of 0.1 and estimating H_0 at each step. Plots showing this test for the cases of linear and step mass correction are given in Figs. 8 and 9, respectively. We find that for the SBF calibration, both step and linear mass corrections give a ∼0.7% decrease in H_0 compared to the H_0 estimated without mass correction (noHM) for any chosen value of M_0 and M_{step}. However, for the SH0ES calibration, while the linear correction gives a ∼1.3% increase for any value of M_0, the step correction gives fluctuating H_0 values when choosing different M_{step} values. At $M_{\mathrm{step}} = 9.7$, we find a decrease of 0.7% in the H_0 value with respect to the noHM calibration, which is consistent with what was found in R16 assuming $M_{\mathrm{step}} = 10$. Table 7 lists the corresponding H_0 values from different cases discussed here.

The mass corrections for both the SBF and SH0ES calibrations has a small effect on the H_0 estimates (ranging between 0.6% and 1.4%). The mass corrections does not resolve the difference among the H_0 estimates from SBF and SH0ES calibrations. The H_0 estimate from the SBF calibration remains smaller than that from the SH0ES calibration.

6. SN Ia distance comparison

In order to understand the difference in the H_0 value derived using the Cepheid and the SBF calibrations, we now focus on

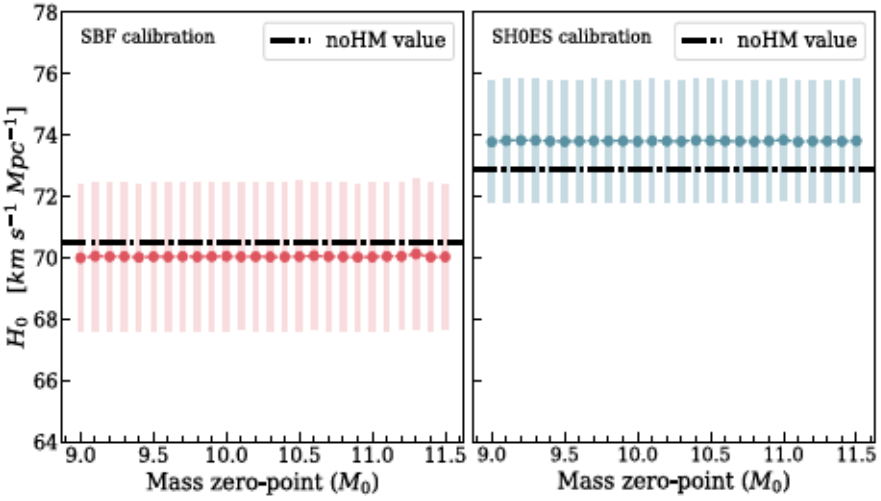

Fig. 8. H_0 values estimated including the linear mass correction in the calibration at different values of M_0. For the SBF calibration (*left panel*), the linear mass correction decreases the value of H_0 by ~0.6% with respect to the H_0 estimated without mass correction (noHM value, shown in dotted black line) for any chosen value of M_0. For the SH0ES calibration (*right panel*), we see an increase of 1.3% from the noHm value. This justifies an arbitrary choice for M_0.

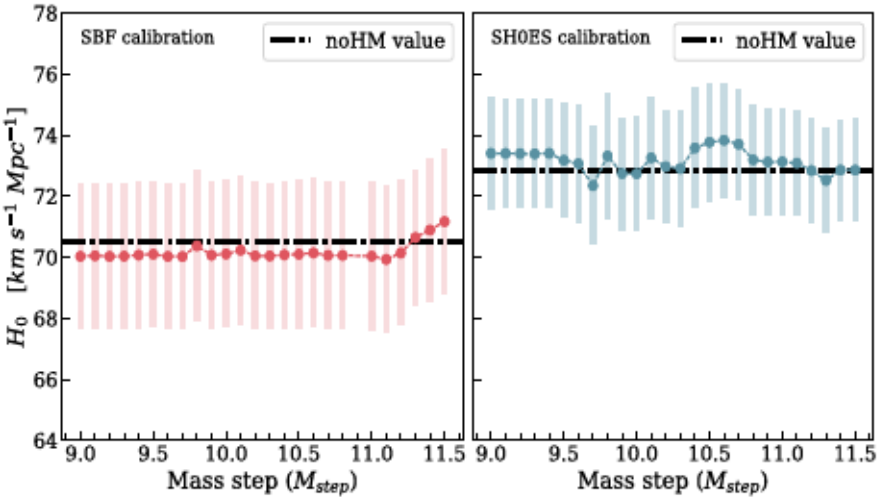

Fig. 9. H_0 values estimated including the step mass correction in the calibration at different values of $M_{\rm step}$. The SBF calibration with a step mass correction decreases the H_0 value by ~0.5% almost consistently at each $M_{\rm step}$ except at the extreme end. However, for the SH0ES calibration, step based correction gives fluctuating values. The lowest value is found at $M_{\rm step} = 9.7$ and is 0.7% lower than the noHM value and the highest is found for $M_{\rm step} = 10.6$, which is 1.4% higher than the noHM value of H_0.

Table 7. Hubble constant values estimated with applying the host mass correction to redshift-cut cosmological sample calibrated with the SBF and SH0ES samples.

Mass	SBF calibration		Cepheid calibration	
correction	H_0	σ_{H_0}	H_0	σ_{H_0}
Linear ($M_0 = 11$)	70.03	2.38	73.78	2.00
Step ($M_{\rm step} = 10$)	70.10	2.39	72.73	1.84
Step ($M_{\rm step} = 9.7$)	70.02	2.38	72.35	1.92
Step ($M_{\rm step} = 10.6$)	70.14	2.42	73.83	1.84
noHM correction	70.50	2.37	72.84	1.66

Notes. The first row shows the results of applying a linear mass correction, and the other rows show a mass step correction as described in the text. The last line shows the values of the H_0 estimated without mass correction for comparison.

the comparison of the SN Ia distance moduli obtained using the two calibrations. Using the luminosity correlation parameters inferred for SBF and SH0ES calibrations (without the host galaxy mass correction), we evaluate the distances for the 96 SNe in the redshift-cut cosmological sample as:

$$\mu = m_B - P^0 - P^1(s_{BV} - 1) - R(m_B - m_V), \quad (15)$$

where the correlation parameter values are given in Table 4. The uncertainty $\sigma_\mu^{\rm SBF/Ceph}$ in the distance modulus of each object is computed via error propagation including the LC fitting errors and the errors in Tripp parameters computed by the Bayesian analysis. We also add the intrinsic variance of the calibrator sample $\sigma_{\rm int,calib}$. Figure 10 shows the comparison between the distance moduli of the SNe obtained using the SBF (x-axis) and Cepheid (y-axis) calibration about a slope-of-unity line. The residuals ($\mu^{\rm Ceph} - \mu^{\rm SBF}$) are plotted in the bottom panel. The distance moduli estimated with the SBF calibration result to be systematically larger than those estimated with Cepheid calibration (as shown in Fig. 10). The different H_0 estimates correspond to a mean difference in distance moduli of 0.07 mag. Adopting the latest LMC distance scale for the SBF and SH0ES calibrators as described in Sect. 4, the mean difference in the distance moduli is found to be 0.066 mag.

In order to examine the origin of this systematic difference, we inspect the SN distances of the two calibration samples (SBF and SH0ES). A direct comparison of distance moduli with SBF and Cepheid techniques requires that SNe Ia happened in galaxies where both SBF and Cepheid distance measurements are available. Only one object SN2012cg among our two calibrator samples satisfy this requirement for which $\mu_{\rm SBF} - \mu_{\rm Cepheid}$ is −0.06 mag. Since this difference is not statistically significant, we compare the SN distance moduli of the SBF and SH0ES samples measured by performing the same analysis as described

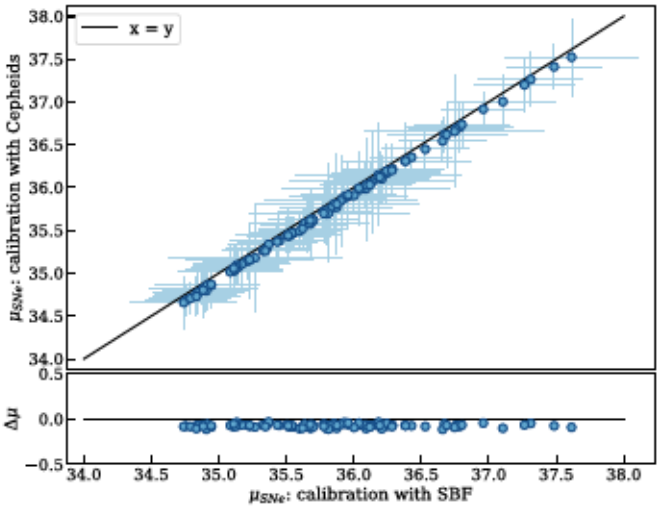

Fig. 10. Distance moduli of the SNe Ia belonging to the redshift-cut cosmological sample estimated using the Cepheid (y-axis) and the SBF (x-axis) as calibrator. The calibration is performed as described in Sect. 3. It does not include the host galaxy mass correction. For a visual comparison, the line $x = y$ is plotted. *Bottom panel*: residual difference among the distances calibrated by Cepheid and SBF, $\Delta\mu = \mu^{\rm Ceph} - \mu^{\rm SBF}$.

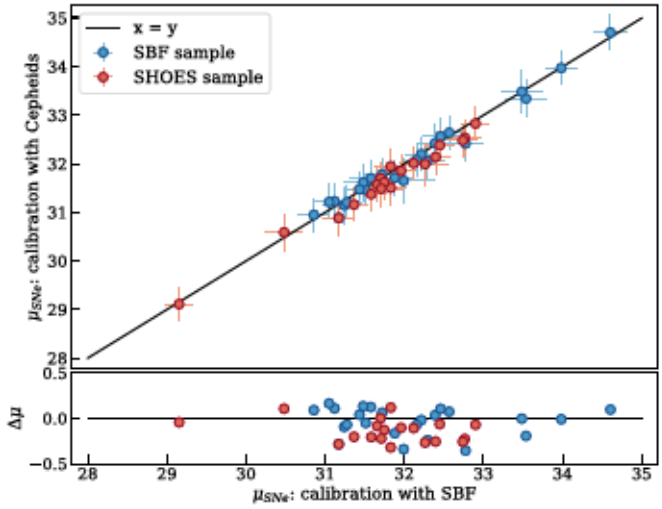

Fig. 11. Distance moduli of the SNe Ia belonging to the two local samples (SBF and SH0ES) estimated using the Cepheid (y-axis) or the SBF (x-axis) as calibrators. The two calibrations used here do not include the cosmological sample in the analysis. It does not include the host galaxy mass correction. For a visual comparison, the line $x = y$ is plotted. *Bottom panel*: residual difference among the distances calibrated by Cepheid and SBF, $\Delta\mu = \mu^{\rm Ceph} - \mu^{\rm SBF}$.

in Sect. 3 but without including the cosmological sample (i.e., only $\mathcal{L}_{\rm calib}$ in the likelihood). Figure 11 shows the comparison of the distance moduli calibrated with the SBF and Cepheids for the two local calibration samples. For SNe of both the SBF and the SH0ES sample, the SBF calibration gives a longer distance scale than the Cepheid calibration, indicating that the difference observed in the distance moduli of the cosmological sample comes directly from intrinsic differences in the local calibration samples.

Ajhar et al. (2001) made a similar comparison using 14 galaxies that host SNe Ia. They compared the SBF distances of these galaxies with the SN distances estimated using the Cepheid calibration by F01, and found them in agreement. In our SBF sample there are nine SNe Ia in common with their paper (for five of them, the SBF measurement used in this paper comes directly from Ajhar et al. 2001). For these nine objects, we find good agreement ($\Delta\mu \sim -0.01$ mag) between the SN distances calibrated with SH0ES Cepheids (performing our analysis using only the local sample) and the SN distances calibrated with Cepheids by Ajhar et al. (2001) that are taken from Table 3, Col. 5 of their paper. This comparison limited to 9/24 galaxies seems to exclude a systematic offset associated with the calibration using SH0ES Cepheids (R16) and HST KP Cepheids (F01).

In Fig. 12 we show a comparison between the directly measured SBF distances ($\mu_{\rm SBF}$, given in Table 1) versus the SN distances estimated using the SBF calibration (left plot) for the SBF sample. In the same figure we also show the plot for the SH0ES sample, where we compare the directly measured Cepheids distances (from R16) with the distances estimated using the Cepheid calibration. In both cases we find a good one-to-one agreement. In comparison to the Cepheids sample, the SBF sample shows a larger scatter (as indicated by $\sigma_{\rm int,calib}$ for SBF).

Figure 13 shows the nearby Hubble diagram for the two calibrator samples, that is, the galaxy recessional velocity versus the distance estimated with SBF (blue data) and with the Cepheids (red data). At such distance scales, the peculiar velocities are significant with respect to the Hubble recessional velocity and need

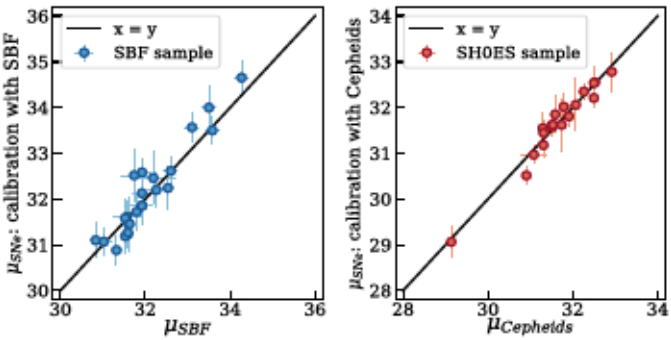

Fig. 12. Distance modulus comparisons of the two local calibration samples. *Left plot*: comparison between directly measured SBF distances ($\mu_{\rm SBF}$, given in Table 1) for the SBF sample, with the SNe distances estimated using the SBF calibration of the cosmological redshift-cut sample of 96 SNe as described in Sect. 3. *Right plot*: similar comparison for the SH0ES sample, comparing the measured Cepheid distances (from R16) with the distances estimated using the Cepheid calibration of the cosmological redshift-cut sample. In both cases we find a good one-to-one agreement.

to be corrected. Here, the recessional velocity of each galaxy is corrected for peculiar velocities with the Cosmic Flow (CF) model following the analysis performed in Carrick et al. (2015). This model takes into account the influence of the large-scale structures in the local Universe. The plot shows that the two samples are equally distributed and that the SBF sample reaches higher distances than the Cepheid one, enabling a larger distance range to calibrate cosmological distances.

7. Discussion

The SBF distances have been directly used to estimate H_0 as proposed for the first time by Ferrarese et al. (2000). This work presents the first attempt to use the SBF measurements to calibrate the peak luminosity of SNe Ia, and thus deriving SN

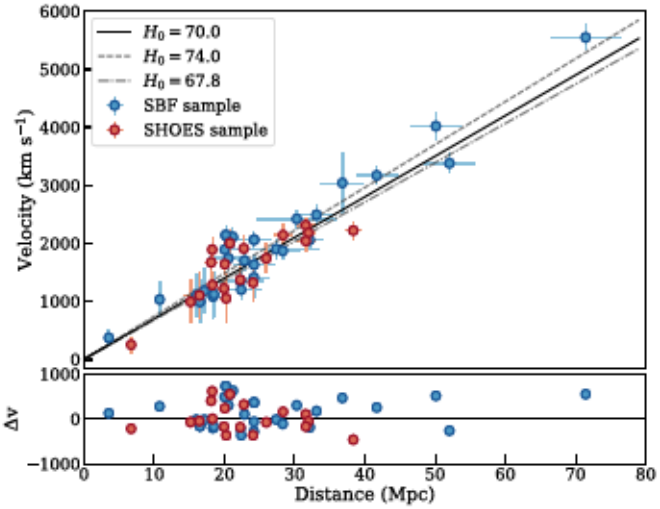

Fig. 13. Nearby Hubble diagram for galaxies with SBF and Cepheid distance measurements. The recessional velocities for all galaxies are corrected for peculiar motions with the CF model following Carrick et al. (2015). As a reference, also shown is the Hubble law for the values of the Hubble constant of $H_0 = 70.0\,\mathrm{km\,s^{-1}\,Mpc^{-1}}$ (solid line), $H_0 = 74.0\,\mathrm{km\,s^{-1}\,Mpc^{-1}}$ (dashed line) and $H_0 = 67.8\,\mathrm{km\,s^{-1}\,Mpc^{-1}}$ (dot-dashed line). *Bottom panel*: residuals for both the SBF and SH0ES samples calculated assuming a H_0 of $70\,\mathrm{km\,s^{-1}\,Mpc^{-1}}$.

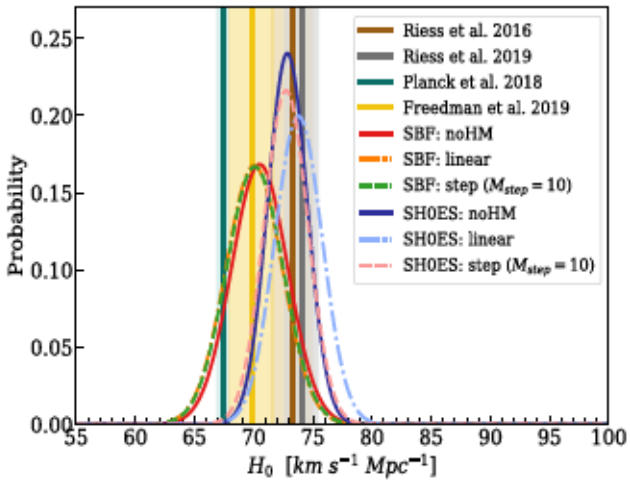

Fig. 14. Posterior distributions of H_0 estimated in this work with the SBF and SH0ES calibrator samples. We give the distributions for noHM analysis (solid line), including a linear mass correction (dot-dashed line) and including a step-mass correction with $M_{\mathrm{step}} = 10$ (dashed line).

distances and the Hubble constant value using this alternative calibration. In our analysis, we found a mean difference of 0.07 mag between the distance moduli of the cosmological samples estimated using the SBF calibration and the ones estimated using the Cepheid calibration (the corresponding difference is 3.3% between the H_0 estimates from them). This difference cannot be accounted for by an identifiable offset on the Cepheid calibration used for the SBF measurements with respect to the SH0ES sample (see discussion on LMC distance and Cepheid P–L relations in Sect. 2 and comparison with Ajhar et al. 2001 in Sect. 6).

Even though we are not able to clearly identify the cause of the difference between the SBF and Cepheid calibrated distances, our results seem to indicate that there are intrinsic differences in SNe Ia hosted in different types of environments, which are not accounted for by applying a simple host-mass correction. The different SN light curve behavior in the two samples could be attributed to differences in their SN Ia progenitors (e.g., Mannucci et al. 2006; Maoz et al. 2014; Livio & Mazzali 2018) since the SBF sample is mainly composed of early E/S0 type galaxies, while the SH0ES sample consists of late-type spiral galaxies. Rigault et al. (2015) showed that SNe Ia in locally star-forming environments are dimmer than SNe Ia hosted in locally passive environments. In this scenario the larger distance moduli given by SBF could be due to SNe Ia exploding in older environments. Considering the general evidence that in early-type galaxies we generally observe older Population II stars while in late-type galaxies we also observe young Population I stars, differences in the evolution of the lightcurve in the first ~50 days of the SN emission could be expected due to the different physical properties and composition of the SN ejecta, which can affect the amount of Fe-peak elements produced in the SN explosion. Another ingredient is how dust extinction influences the SN Ia light curves. Comprehensive lightcurve modeling suggests that the main source of intrinsic scatter for the observed SN Ia emission is from the extinction parameter R, which reflects variation of the dust around the SNe Ia (Brout & Scolnic 2020), although a recent detailed work on NIR SN Ia lightcurves seems to exclude the dust as main driver of the host galaxy and SN Ia luminosity correlation (Ponder et al. 2020). In line with these results, we find slightly lower ($\Delta R \sim 0.15$) value for the SBF sample average extinction parameter R with respect to the SH0ES sample, see Table 5. However, this is not enough to explain the observed difference in the cosmological samples calibrated with the two methods, given that the average color (m_B–m_V) values of the three samples in this work are much smaller than 1 mag. The mean color for the SBF sample is 0.09 mag, for the SH0ES sample it is 0.07 mag, and for the cosmological sample it is 0.1 mag.

7.1. Hubble tension

Our final H_0 value estimated from SBF calibration using 24 SNe Ia applied to the redshift-cut cosmological sample is $H_0 = 70.50 \pm 2.37\,(\mathrm{stat.}) \pm 3.38\,(\mathrm{sys.})\,\mathrm{km\,s^{-1}\,Mpc^{-1}}$. This H_0 value, obtained with SBF calibration stands ~1.3σ away from both the *Planck* H_0 estimate of the early Universe (Planck Collaboration VI 2020) and the SH0ES program H_0 estimate (Riess et al. 2019), when we only take into account the statistical errors. Our H_0 value is in good agreement with the recent estimate by Freedman et al. (2019) based on the TRGB calibration of SNe Ia. As pointed out by Freedman et al. (2020), TRGB stars populate the gas- and dust- free halos of the host galaxy in contrast to the Cepheids, which are found in the higher-surface-brightness disk regions. TRGB stars sample environments more similar to the SBF galaxies. Figure 14 summarizes the H_0 measurements in the present work for the various cases of noHM and HM corrections with SBF and SH0ES calibrators, and shows their comparison with measurements by Planck Collaboration VI (2020), Freedman et al. (2019), and Riess et al. (2016, 2019).

7.2. Perspectives for the SN Ia SBF calibration

The present work uses both ground based and HST SBF optical data. In the future, we expect major improvements in this regard by using dedicated observations by the *James Webb* Space Telescope (JWST). The SBF method works better in the NIR because the main source of the brightness fluctuations comes

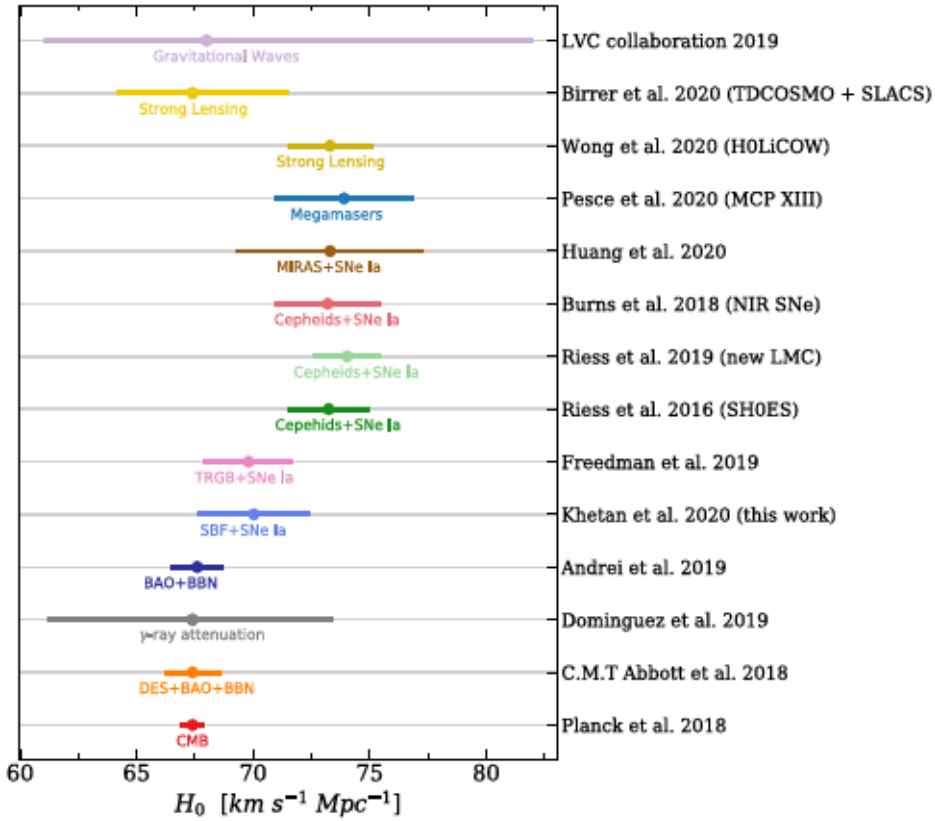

Fig. 15. Compilation of Hubble constant values obtained using different observations and techniques from the recent literature including the value from this work. The literature references are written on the *y*-axis. Two independent estimates from early Universe (Planck Collaboration XIII 2016; Abbott et al. 2018) are shown at the bottom. The next is an estimate using extragalactic background light γ ray attenuation (Domínguez et al. 2019) and another from BAO at all redshifts + BBN estimate (Cuceu et al. 2019). Then we show measurements from SNe Ia calibrated with TRGB (Freedman et al. 2019), SNe Ia calibrated with Cepheids (SH0ES sample, Riess et al. 2016, 2019), using near-infrared (NIR) filters (Burns et al. 2018) and SNe Ia with Mira variables (Huang et al. 2020). Then we show the H_0 values estimated using 6 masers in the Hubble flow (Pesce et al. 2020). The next H_0 value shown is inferred via gravitational lensing time delays using six lensed quasars (Wong et al. 2020) and a more recent value obtained using 40 strong lenses (Birrer et al. 2020). Finally we shows the H_0 derived with gravitational-wave signals from binary compact object mergers (Abbott et al. 2019).

from red giant branch stars which are brighter at redder wavelengths (Blakeslee et al. 2010) and less affected by dust extinction. The red giants are excellent targets for JWST. However, the SBF calibration is presently not well-constrained in the NIR bands compared to the optical ones (Jensen et al. 2015). SBF offers a complementary tool to calibrate SN Ia luminosity with respect to the Cepheids by sampling a set of different type of host galaxy environment. Although SBF is currently a secondary distance indicator, as it is dependent on Cepheid calibration, the theoretical calibrations that will eventually make it an independent technique in the distance ladder (Cantiello et al. 2005) are improving.

Furthermore, SBF represents an experimental methodology that is able to anchor the distance ladder up to larger distances with respect to the Cepheid calibrations (see e.g., Fig. 13). As SNe Ia are rare events, reaching larger distances will provide more galaxies that host a SN Ia, giving us larger number of calibrators, which is very important to decrease the statistical errors and reach a percent level precision goal. In this work, the measured scatter in the *B*-band absolute magnitudes of the fiducial calibrating sample is 0.27 mag. With 24 SBF calibrators, the uncertainty in mean absolute magnitude is 0.05 mag, which corresponds to about 2.5% uncertainty in distance. While the SBF sample is expected to largely increase with the future instruments and newly discovered SNe Ia, the increase in the number of Cepheid calibrators will be limited by the smaller distance necessary for Cepheid measurements, and thus the smaller number of galaxies possibly hosting a SN explosion. The importance of having a larger number of SN Ia calibrators is also highlighted in Freedman et al. (2019), and by Huang et al. (2020) where Mira variables have been used to calibrate SNe Ia and to measure the Hubble constant.

8. Conclusion and perspectives

The primary goal of this work is to show the potential of the SBF method to provide an alternative distance scale for the local Universe aimed at calibrating the absolute magnitudes of SNe Ia and measuring the Hubble constant. We built a set of 24 SNe Ia calibrators that have distance measurements to their hosts, mostly early-type galaxies, obtained with the SBF technique. We applied the SBF calibration to a sample of 96 SNe Ia with redshifts between $z = 0.02$ and $z = 0.075$ (obtained from the Combined Pantheon Sample) and derived a value of $H_0 = 70.50 \pm 2.37\,(\mathrm{stat.}) \pm 3.38\,(\mathrm{sys.})\,\mathrm{km\,s^{-1}\,Mpc^{-1}}$ (i.e., 3.4% stat., 4.8% sys.). This value lies in between the value obtained with SNe Ia calibrated with Cepheids and that inferred from the analysis of the CMB; it is consistent with both of them within the errors.

We found a systematic difference of 0.07 mag among the distances estimated using the SBF calibration and the ones using the Cepheid calibration (see Fig. 10). This accounts for the ∼3.3% smaller H_0 value obtained using SBF calibration with respect the one using the SH0ES sample as calibrator. This also explains the ∼5% larger H_0 value of Riess et al. (2019), which uses SH0ES sample as calibrators, compared to the SBF.

Although we are not able to completely exclude a hidden primary calibration offset, the observed difference could be attributed to the different host properties of the SBF and SH0ES calibrator samples. Cepheids are usually observed in late-type galaxies while SBF can be measured only for homogeneous, passive environments, such as early-type and lenticular S0 galaxies. In terms of SNe Ia, different host galaxy types can translate into: (a) a difference in the intrinsic dust reddening or immediate extinction, possibly due to the presence of local dense circumstellar medium; (b) a different stellar population for the underlying SN progenitor, for example, due to the existence of multiple channels for the formation of the binary systems leading to a SN Ia explosion (Mannucci et al. 2006; Foley et al. 2020); (c) a difference in the metallicity or chemical composition of the underlying progenitor, which can lead to a different light curve evolution (Maoz et al. 2014; Livio & Mazzali 2018). At the moment we can neither confirm nor exclude any of these possible scenarios. We believe that additional observations and analysis, in particular at NIR wavelengths, are needed to shed light on this problem. Compared to optical LCs, NIR SNe Ia LCs have a narrow luminosity distribution and are less sensitive to host galaxy dust extinction (Avelino et al. 2019). Moreover, the possibility of investigating the immediate environments, using, for example, integral field spectrographs, of nearby SNe Ia can provide important clues to the fundamental physical properties of the circumstellar gas surrounding SN progenitors.

Our analysis shows that applying a correction for the host-galaxy stellar mass in the luminosity calibration relation does not reduce or correct for the possible SN Ia luminosity dependence on galaxy types (see Sect. 5). This suggests the need for alternative parameter(s) that could account for the variation in the luminosity of SNe Ia hosted in different environments. This is particularly timely taking into account the upcoming observations of innovative observatories (e.g., *Vera C. Rubin* Observatory, JWST) that are expected to increase the number of detected SNe Ia, in particular at larger redshift.

Today the value of local Universe H_0 is known with an uncertainty of less than 10%. However, Fig. 15, which shows the current status of H_0 estimates with different methodologies, reveals the existence of a dichotomy in the H_0 measurements; a first group of measures characterized by a central value below 70 km s^{-1} Mpc^{-1}, and a second one centered above 73 km s^{-1} Mpc^{-1}. The current "tension" on the H_0 measurements is not only limited to CMB and Cepheid measurements but instead involves a dozen of different methods, mostly independent of each other. Our results together with the other data reported in Fig. 15 suggest that there is a certain margin to interpret the discrepant results in terms of systematics while relaxing the quest for new physics.

Acknowledgements. We are grateful to Christopher Burns for his very useful comments and help with Light curve fitting using SNooPy. We thank the SN group at the Observatory of Padova, INAF for hosting NK as short-term visitor and for the valuable discussions on the nature of SNe Ia and their observation. We also extend our thanks to the researchers at DARK, Copenhagen for hosting NK as short-term visitor and discussing various details of the analysis and comments on the manuscript. NK is grateful to Jeff Cooke and CAS (Swinburne University) Melbourne for hosting her as a visiting PhD student. NK would further like to acknowledge helpful discussions with Chris Blake and Suhail Dhawan. MB, EB, EC, and MC acknowledge financial support from MIUR (PRIN 2017 grant 20179ZF5KS). This work was supported by a VILLUM FONDEN Investigator grant to JH (project number 16599) and by a VILLUM FONDEN Young Investigator grant to CG (project number 25501). This project is funded by the Danish Council for Independent Research under the project 'Fundamentals of Dark Matter Structures', DFF – 6108-00470. We would also like to extend our thanks to Adam Riess and Dan Scolnic for useful discussions. We are grateful to the referee for their comments.

References

Abbott, B. P., Abbott, R., Abbott, T. D., et al. 2017, Nature, 551, 85
Abbott, T. M. C., Abdalla, F. B., Annis, J., et al. 2018, MNRAS, 480, 3879
Abbott, B. P., Abbott, R., Abbott, T. D., et al. 2019, ArXiv e-prints [arXiv:1908.06060]
Ajhar, E. A., Tonry, J. L., Blakeslee, J. P., Riess, A. G., & Schmidt, B. P. 2001, ApJ, 559, 584
Alam, S., Ata, M., Bailey, S., et al. 2017, MNRAS, 470, 2617
Altavilla, G., Fiorentino, G., Marconi, M., et al. 2004, MNRAS, 349, 1344
Arendse, N., Wojtak, R. J., Agnello, A., et al. 2020, A&A, 639, A57
Aubourg, É., Bailey, S., Bautista, J. E., et al. 2015, Phys. Rev. D, 92, 123516
Avelino, A., Friedman, A. S., Mandel, K. S., et al. 2019, ApJ, 887, 106
Bennett, C. L., Larson, D., Weiland, J. L., et al. 2013, ApJS, 208, 20
Bernal, J. L., Verde, L., & Riess, A. G. 2016, JCAP, 2016, 019
Betoule, M., Kessler, R., Guy, J., et al. 2014, A&A, 568, A22
Birrer, S., Treu, T., Rusu, C. E., et al. 2019, MNRAS, 484, 4726
Birrer, S., Shajib, A. J., Galan, A., et al. 2020, A&A, 643, A165
Biscardi, I., Raimondo, G., Cantiello, M., & Brocato, E. 2008, ApJ, 678, 168
Blakeslee, J. P. 2012, Ap&SS, 341, 179
Blakeslee, J. P., Ajhar, E. A., & Tonry, J. L. 1999, in Distances from Surface Brightness Fluctuations, eds. A. Heck, & F. Caputo, Astrophys. Space Sci. Lib., 237, 181
Blakeslee, J. P., Vazdekis, A., & Ajhar, E. A. 2001, MNRAS, 320, 193
Blakeslee, J. P., Lucey, J. R., Tonry, J. L., et al. 2002, MNRAS, 330, 443
Blakeslee, J. P., Jordán, A., Mei, S., et al. 2009, ApJ, 694, 556
Blakeslee, J. P., Cantiello, M., Mei, S., et al. 2010, ApJ, 724, 657
Brocato, E., Capaccioli, M., & Condelli, M. 1998, Mem. Soc. Astron. It., 69, 155
Brout, D., & Scolnic, D. 2020, ArXiv e-prints [arXiv:2004.10206]
Brown, P. J., Breeveld, A. A., Holland, S., Kuin, P., & Pritchard, T. 2014, Ap&SS, 354, 89
Burns, C. R., Stritzinger, M., Phillips, M. M., et al. 2011, AJ, 141, 19
Burns, C. R., Stritzinger, M., Phillips, M. M., et al. 2014, ApJ, 789, 32
Burns, C. R., Parent, E., Phillips, M. M., et al. 2018, ApJ, 869, 56
Cadonau, R., & Leibundgut, B. 1990, A&AS, 82, 145
Cantiello, M., Raimondo, G., Brocato, E., & Capaccioli, M. 2003, AJ, 125, 2783
Cantiello, M., Blakeslee, J. P., Raimondo, G., et al. 2005, ApJ, 634, 239
Cantiello, M., Blakeslee, J., Raimondo, G., Brocato, E., & Capaccioli, M. 2007, ApJ, 668, 130
Cantiello, M., Grado, A., Blakeslee, J. P., et al. 2013, A&A, 552, A106
Cantiello, M., Jensen, J. B., Blakeslee, J. P., et al. 2018a, ApJ, 854, L31
Cantiello, M., Blakeslee, J. P., Ferrarese, L., et al. 2018b, ApJ, 856, 126
Carrick, J., Turnbull, S. J., Lavaux, G., & Hudson, M. J. 2015, MNRAS, 450, 317
Cole, S., Percival, W. J., Peacock, J. A., et al. 2005, MNRAS, 362, 505
Conley, A., Guy, J., Sullivan, M., et al. 2011, ApJS, 192, 1
Contreras, C., Hamuy, M., Phillips, M. M., et al. 2010, AJ, 139, 519
Cuceu, A., Farr, J., Lemos, P., & Font-Ribera, A. 2019, JCAP, 2019, 044
Dhawan, S., Jha, S. W., & Leibundgut, B. 2018, A&A, 609, A72
Dhawan, S., Brout, D., Scolnic, D., et al. 2020, ApJ, 894, 54
Domínguez, A., Wojtak, R., Finke, J., et al. 2019, ApJ, 885, 137
Eisenstein, D. J., Zehavi, I., Hogg, D. W., et al. 2005, ApJ, 633, 560
Ferrarese, L., Mould, J. R., Kennicutt, R. C., Jr., et al. 2000, ApJ, 529, 745
Folatelli, G., Phillips, M. M., Burns, C. R., et al. 2010, AJ, 139, 120
Foley, R. J., & Kasen, D. 2011, ApJ, 729, 55
Foley, R. J., Hoffmann, S. L., Macri, L. M., et al. 2020, MNRAS, 491, 5991
Freedman, W. L., & Madore, B. F. 2010, ARA&A, 48, 673
Freedman, W. L., Madore, B. F., Gibson, B. K., et al. 2001, ApJ, 553, 47
Freedman, W. L., Burns, C. R., Phillips, M. M., et al. 2009, ApJ, 704, 1036
Freedman, W. L., Madore, B. F., Scowcroft, V., et al. 2012, ApJ, 758, 24
Freedman, W. L., Madore, B. F., Hatt, D., et al. 2019, ApJ, 882, 34
Freedman, W. L., Madore, B. F., Hoyt, T., et al. 2020, ApJ, 891, 57
Gaia Collaboration (Brown, A. G. A., et al.) 2018, A&A, 616, A1
Gall, C., Stritzinger, M. D., Ashall, C., et al. 2018, A&A, 611, A58
Guillochon, J., Parrent, J., Kelley, L. Z., & Margutti, R. 2017, ApJ, 835, 64
Gupta, R. R., D'Andrea, C. B., Sako, M., et al. 2011, ApJ, 740, 92
Hamuy, M., Phillips, M. M., Maza, J., et al. 1991, AJ, 102, 208

Hamuy, M., Phillips, M. M., Suntzeff, N. B., et al. 1996, AJ, 112, 2408
Hayden, B. T., Gupta, R. R., Garnavich, P. M., et al. 2013, ApJ, 764, 191
Hicken, M., Challis, P., Jha, S., et al. 2009a, ApJ, 700, 331
Hicken, M., Wood-Vasey, W. M., Blondin, S., et al. 2009b, ApJ, 700, 1097
Hicken, M., Challis, P., Kirshner, R. P., et al. 2012, ApJS, 200, 12
Hill, J. C., McDonough, E., Toomey, M. W., & Alexander, S. 2020, Phys. Rev. D, 102, 043507
Hoffmann, S. L., Macri, L. M., Riess, A. G., et al. 2016, ApJ, 830, 10
Howell, D. A. 2001, ApJ, 554, L193
Hsiao, E. Y., Conley, A., Howell, D. A., et al. 2007, ApJ, 663, 1187
Huang, C. D., Riess, A. G., Yuan, W., et al. 2020, ApJ, 889, 5
Jensen, J. B., Tonry, J. L., Thompson, R. I., et al. 2001, ApJ, 550, 503
Jensen, J. B., Tonry, J. L., Barris, B. J., et al. 2003, ApJ, 583, 712
Jensen, J. B., Blakeslee, J. P., Gibson, Z., et al. 2015, ApJ, 808, 91
Jha, S., Kirshner, R. P., Challis, P., et al. 2006, AJ, 131, 527
Kang, Y., Lee, Y.-W., Kim, Y.-L., Chung, C., & Ree, C. H. 2020, ApJ, 889, 8
Kelly, P. L., Hicken, M., Burke, D. L., Mandel, K. S., & Kirshner, R. P. 2010, ApJ, 715, 743
Kennicutt, R. C., Jr., Stetson, P. B., Saha, A., et al. 1998, ApJ, 498, 181
Knox, L., & Millea, M. 2020, Phys. Rev. D, 101, 043533
Lampeitl, H., Smith, M., Nichol, R. C., et al. 2010, ApJ, 722, 566
Li, W., Filippenko, A. V., Gates, E., et al. 2001, PASP, 113, 1178
Livio, M., & Mazzali, P. 2018, Phys. Rep., 736, 1
Macaulay, E., Nichol, R. C., Bacon, D., et al. 2019, MNRAS, 486, 2184
Madore, B. F., & Freedman, W. L. 1991, PASP, 103, 933
Maeda, K., Leloudas, G., Taubenberger, S., et al. 2011, MNRAS, 413, 3075
Mannucci, F., Della Valle, M., & Panagia, N. 2006, MNRAS, 370, 773
Maoz, D., Mannucci, F., & Nelemans, G. 2014, ARA&A, 52, 107
Marín-Franch, A., & Aparicio, A. 2006, A&A, 450, 979
Mei, S., Scodeggio, M., Silva, D. R., & Quinn, P. J. 2003, A&A, 399, 441
Mei, S., Blakeslee, J. P., Tonry, J. L., et al. 2005, ApJ, 625, 121
Mörtsell, E., & Dhawan, S. 2018, JCAP, 2018, 025
Mosher, J., Guy, J., Kessler, R., et al. 2014, ApJ, 793, 16
Neill, J. D., Sullivan, M., Howell, D. A., et al. 2009, ApJ, 707, 1449
Perlmutter, S., Gabi, S., Goldhaber, G., et al. 1997, ApJ, 483, 565
Pesce, D. W., Braatz, J. A., Reid, M. J., et al. 2020, ApJ, 891, L1
Phillips, M. M. 1993, ApJ, 413, L105
Phillips, M. M., Contreras, C., Hsiao, E. Y., et al. 2019, PASP, 131, 014001
Pietrzyński, G., Graczyk, D., Gieren, W., et al. 2013, Nature, 495, 76
Pietrzyński, G., Graczyk, D., Gallenne, A., et al. 2019, Nature, 567, 200
Planck Collaboration XIII. 2016, A&A, 594, A13
Planck Collaboration VI. 2020, A&A, 641, A6
Ponder, K. A., Wood-Vasey, W. M., Weyant, A., et al. 2020, ApJ, submitted [arXiv:2006.13803]
Pruzhinskaya, M., Novinskaya, A., Pauna, N., & Rosnet, P. 2020, MNRAS, 499, 5121
Raimondo, G., Brocato, E., Cantiello, M., & Capaccioli, M. 2005, AJ, 130, 2625
Richmond, M., & Vietje, B. 2017, J. Am. Assoc. Var. Star Obs. (JAAVSO), 45, 65
Richmond, M. W., Treffers, R. R., Filippenko, A. V., et al. 1995, AJ, 109, 2121
Riess, A. G., Press, W. H., & Kirshner, R. P. 1996, ApJ, 473, 88
Riess, A. G., Kirshner, R. P., Schmidt, B. P., et al. 1999, AJ, 117, 707
Riess, A. G., Li, W., Stetson, P. B., et al. 2005, ApJ, 627, 579
Riess, A. G., Macri, L., Casertano, S., et al. 2011, ApJ, 730, 119
Riess, A. G., Macri, L. M., Hoffmann, S. L., et al. 2016, ApJ, 826, 56
Riess, A. G., Casertano, S., Yuan, W., Macri, L. M., & Scolnic, D. 2019, ApJ, 876, 85
Rigault, M., Copin, Y., Aldering, G., et al. 2013, A&A, 560, A66
Rigault, M., Aldering, G., Kowalski, M., et al. 2015, ApJ, 802, 20
Roman, M., Hardin, D., Betoule, M., et al. 2018, A&A, 615, A68
Salvatier, J., Wiecki, T. V., & Fonnesbeck, C. 2016, PeerJ Comput. Sci., 2, e55
Sandage, A., Tammann, G. A., Saha, A., et al. 2006, ApJ, 653, 843
Schlafly, E. F., & Finkbeiner, D. P. 2011, ApJ, 737, 103
Scolnic, D., Casertano, S., Riess, A., et al. 2015, ApJ, 815, 117
Scolnic, D. M., Jones, D. O., Rest, A., et al. 2018, ApJ, 859, 101
Silverman, J. M., Foley, R. J., Filippenko, A. V., et al. 2012, MNRAS, 425, 1789
Skrutskie, M. F., Cutri, R. M., Stiening, R., et al. 2006, AJ, 131, 1163
Sorce, J. G., Courtois, H. M., Tully, R. B., et al. 2013, ApJ, 765, 94
Stritzinger, M., Burns, C. R., Phillips, M. M., et al. 2010, AJ, 140, 2036
Stritzinger, M. D., Phillips, M. M., Boldt, L. N., et al. 2011, AJ, 142, 156
Sullivan, M., Conley, A., Howell, D. A., et al. 2010, MNRAS, 406, 782
Suyu, S. H., Bonvin, V., Courbin, F., et al. 2017, MNRAS, 468, 2590
Tody, D. 1986, in The IRAF Data Reduction and Analysis System, ed. D. L. Crawford, SPIE Conf. Ser., 627, 733
Tonry, J., & Schneider, D. P. 1988, AJ, 96, 807
Tonry, J. L., Dressler, A., Blakeslee, J. P., et al. 2001, ApJ, 546, 681
Tripp, R. 1998, A&A, 331, 815
Udalski, A., Szymanski, M., Kubiak, M., et al. 1999, Acta Astron., 49, 201
Verde, L., Treu, T., & Riess, A. G. 2019, Nat. Astron., 3, 891
Vinkó, J., Ordasi, A., Szalai, T., et al. 2018, PASP, 130, 064101
Visser, M. 2004, Classical Quantum Gravity, 21, 2603
Weinberg, S. 1972, Gravitation and Cosmology: Principles and Applications of the General Theory of Relativity (Wiley-VCH), 688
Wen, X.-Q., Wu, H., Zhu, Y.-N., et al. 2013, MNRAS, 433, 2946
Wong, K. C., Suyu, S. H., Chen, G. C. F., et al. 2020, MNRAS, 498, 1420
Yuan, W., Riess, A. G., Macri, L. M., Casertano, S., & Scolnic, D. M. 2019, ApJ, 886, 61

Appendix A: Light curve fitting with SNooPy

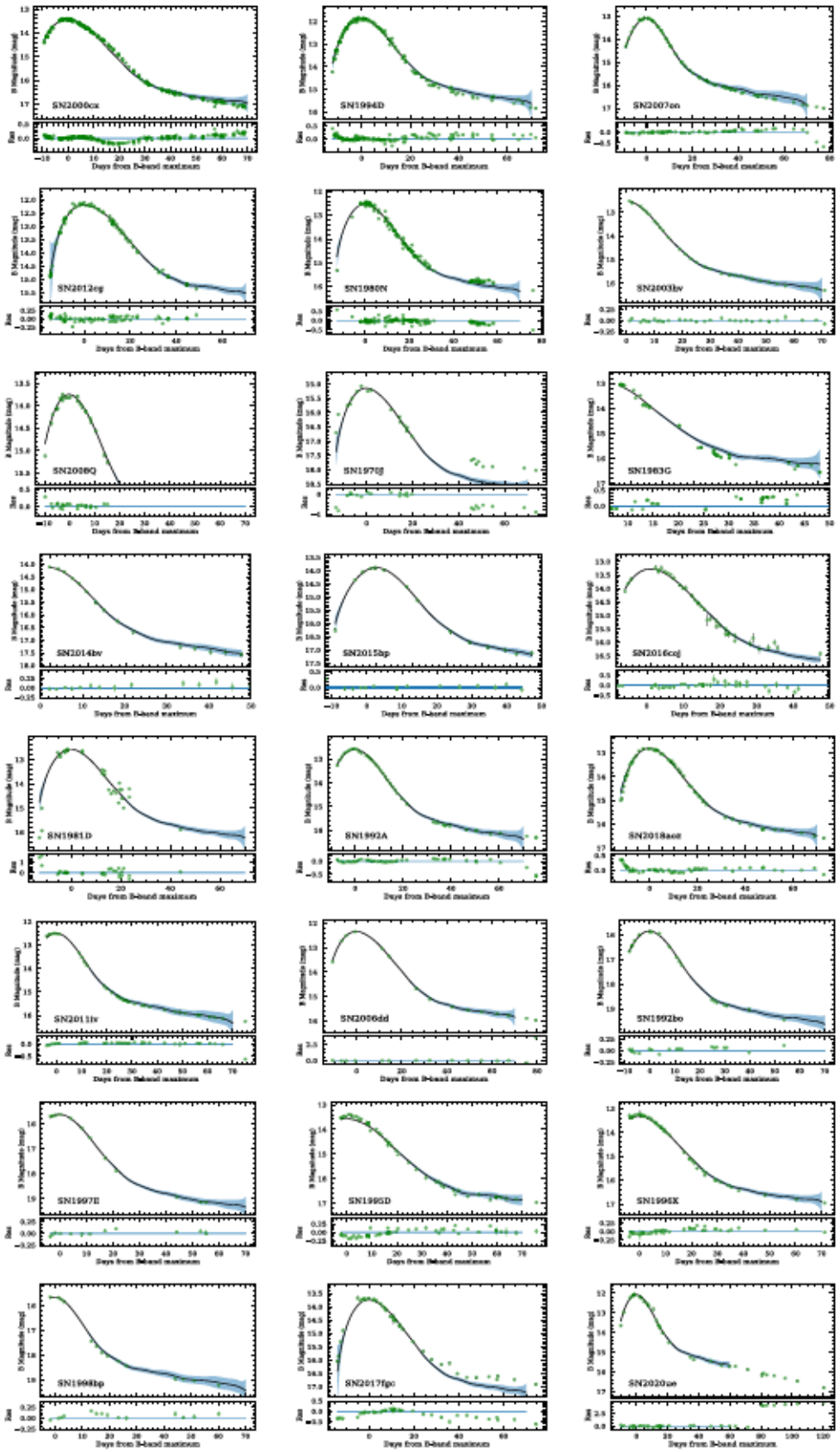

Fig. A.1. *B*-band LC fits of the 24 SNe Ia in the SBF calibrator sample. The fits are done using SNooPy.

Table A.1. Literature references for the optical photometry data of the SNe Ia in the SBF calibrator sample.

Supernova	Host galaxy	Photometry reference
SN2000cx	NGC 524	Li et al. (2001)
SN1994D	NGC 4526	Richmond et al. (1995)
SN2007on	NGC 1404	Stritzinger et al. (2011)
SN2012cg	NGC 4424	Vinkó et al. (2018)
SN1980N	NGC 1316	Hamuy et al. (1991)
SN2003hv	NGC 1201	Silverman et al. (2012)
SN2008Q	NGC 524	Brown et al. (2014)
SN1970J	NGC 7619	Cadonau & Leibundgut (1990)
SN1983G	NGC 4753	Cadonau & Leibundgut (1990)
SN2014bv	NGC 4386	Brown et al. (2014)
SN2015bp	NGC 5839	Brown et al. (2014)
SN2016coj	NGC 4125	Richmond & Vietje (2017)
SN1981D	NGC 1316	Hamuy et al. (1991)
SN1992A	NGC 1380	Altavilla et al. (2004)
SN2018aoz	NGC 3923	Ni et al. (in prep.)
SN2011iv	NGC 1404	Gall et al. (2018)
SN2006dd	NGC 1316	Stritzinger et al. (2010)
SN1992bo	E352−057	Hamuy et al. (1996)
SN1997E	NGC 2258	Jha et al. (2006)
SN1995D	NGC 2962	Riess et al. (1999)
SN1996X	NGC 5061	Riess et al. (1999)
SN1998bp	NGC 6495	Jha et al. (2006)
SN2017fgc	NGC 0474	Burke et al. (in prep.)
SN2020ue	NGC 4636	Khetan et al. (in prep.)

Appendix B: Host galaxy stellar-mass evaluation

The stellar mass of the host galaxies of the two calibrator samples, SBF and SH0ES and the cosmological sample are evaluated using the approach described in the following. The mass for each galaxy is determined using the 2MASS extended source catalog (Skrutskie et al. 2006). We use the K_s-band magnitude for each galaxy and correct it for the extinction. Then, assuming a constant mass-to-light ratio, the stellar mass of the host galaxy is evaluated using an empirical relation derived by Wen et al. (2013):

$$\log_{10}\left(\frac{M_\star}{M_\odot}\right) = (-0.498 \pm 0.002) + (1.105 \pm 0.001) \times \log_{10}\left(\frac{\nu L_\nu(K_s)}{L_\odot}\right), \quad \text{(B.1)}$$

where $L_\nu(K_s)$ is the K_s-band luminosity and 1.105 is the mass-to-light ratio. However, the calculation of $L_\nu(K_s)$ requires knowledge of the distance modulus of the galaxy and hence it introduces a covarience in host mass with the estimated distances (Hubble residual) and should be dealt carefully. Solving the above equation by translating $L_\nu(K_s)$ into μ, one finds that $\log_{10}(M_\star/M_\odot) \propto 0.4\mu$, and therefore we include $0.4\delta\mu^2$ error in our calibration calculations where $\delta\mu$ is the error on the distance modulus. To estimate the error on the stellar mass, we use the standard error propagation. For the SH0ES calibrator sample, two galaxies, NGC 4038 and UGC 9391 (corresponding to SN2007sr and SN2003du, respectively) are not in the 2MASS catalog. For their mass calculation we evaluate the magnitude directly from the K_s-band images. We first flag the foreground stars and replace with random neighboring background pixels using imedit in IRAF (Tody 1986), and then we subtract the sky background. The total flux within an ellipse of appropriate size is measured, which is then converted to stellar mass using the same method and mass-to-light ratio as described above.